



Late Paleozoic supradetachment basin configuration in the southwestern Barents Sea—Intrabasement seismic facies of the Fingerdjupet Subbasin

Julie L. S. Gresseth¹  | Alvar Braathen²  | Christopher S. Serck²  |
Jan Inge Faleide^{2,3}  | Per Terje Osmundsen^{1,4} 

¹Department of Geoscience and Petroleum, NTNU, Trondheim, Norway

²Department of Geosciences, University of Oslo, Oslo, Norway

³Research Centre for Arctic Petroleum Exploration (ARCEX), University of Tromsø, Tromsø, Norway

⁴Department of Arctic Geology, University Centre in Svalbard (UNIS), Longyearbyen, Norway

Correspondence

Julie L. S. Gresseth, Department of Geoscience and Petroleum, NTNU, S. P. Andersens vei 15A, 7031 Trondheim, Norway.

Email: julie.gresseth@ntnu.no

Funding information

Norges Forskningsråd, Grant/Award Number: 295208

Abstract

Late to post-Caledonian, Devonian extension remains unresolved in the SW Barents Sea, despite considerable knowledge from onshore Norway, East Greenland and Svalbard. We analyse intrabasement seismic facies in high-resolution 3D and reprocessed 2D data to investigate evidence for Caledonian deformation and post-Caledonian detachment faulting in the central SW Barents Sea. These results are compared to published potential field models and analogue field studies from onshore Svalbard and Bjørnøya, substantiating that structures inherited from post-orogenic extension influenced the Late Paleozoic and Mesozoic basin evolution. The Late Paleozoic Fingerdjupet Subbasin is underlain by a NNE-striking, ESE-dipping extensional detachment fault that records a minimum eastwards displacement of 22 km. The detachment fault and associated shear zone(s) separate post-orogenic metamorphic core complexes from the syn-tectonic deposits of a presumed Devonian supradetachment basin. Spatial variability in isostatically induced doming likely governed Devonian basin configurations. Pronounced footwall corrugations and faults splaying from the detachment indicate eastward extensional transport. This ultimately led to two interacting but subsequent, east-stepping detachments. Local reactivation of the detachment systems controlled the extent of Carboniferous carbonate and evaporite basins in the Bjarmeland Platform area. Further, the Mesozoic Terningen Fault Complex and Randi Fault Set testify to how the inherited Devonian structural template continued to control spatial localisation and extent of rift structures during subsequent periods of extensional faulting in the Fingerdjupet Subbasin.

KEYWORDS

Caledonian deformation, core complex exhumation, detachment faulting, Devonian sedimentation, intrabasement seismic facies, supradetachment basin, SW Barents Sea

This is an open access article under the terms of the Creative Commons Attribution License, which permits use, distribution and reproduction in any medium, provided the original work is properly cited.

© 2021 The Authors. *Basin Research* published by International Association of Sedimentologists and European Association of Geoscientists and Engineers and John Wiley & Sons Ltd.

1 | INTRODUCTION

Recent interest in basement properties has been inspired by discoveries of hydrocarbons in fractured and weathered crystalline basement. In many areas, resolving the nature and 3D geometry of offshore intrabasement structures has become an important aspect of hydrocarbon exploration (Cuong & Warren, 2009; Lenhart et al., 2019; Trice et al., 2019). Several works focus on the evolution and geometry of basin-bounding normal faults that reactivate basement fabrics, controlled by lithological composition and pre-existing structures (Lenhart et al., 2019; Naliboff et al., 2020; Osmundsen & Péron-Pinvidic, 2018; Phillips et al., 2016; Serck & Braathen, 2019). Despite its importance, basement composition and possible heterogeneity have historically been omitted in basin modelling and in tectono-stratigraphic models of rift development.

Few and inconsistent studies target the composition and location of intrabasement structures in the SW Barents Sea. A variety of works describe deep-imaging by 2D seismic reflection profiles (e.g. Gudlaugsson et al., 1998), seismic refraction data (e.g. Breivik et al., 2005) and regional potential field data and modelling (Gernigon & Brönnner, 2012; Gernigon et al., 2014; Olesen et al., 2010). Reports from field studies in mainland Norway (e.g. Andersen et al., 1994, 1999; Braathen et al., 2000, 2002; Osmundsen et al., 2003, 2006), Northern Norway (Koehl et al., 2018), Bjørnøya (Braathen et al., 1999) and Svalbard (e.g. Bælum & Braathen, 2012; Bergh et al., 2011; Braathen et al., 2018) are of limited value in the central SW Barents Sea, as uncertainty increases with distance from the on-shore study areas. Also, there is a lack of continuous data coverage between the study area and the nearest outcrops at Bjørnøya.

For this study, we constrain the nature, composition and 3D architecture of crystalline basement to lower cover succession in the Fingerdjupet Subbasin-Bjarmeland Platform region (Figure 1), by utilising recently reprocessed, high-resolution seismic reflection data in combination with potential field and seismic refraction data. Our approach is similar to studies of intrabasement seismic reflection studies in the North Sea (e.g. Fazlikhani et al., 2017; Lenhart et al., 2019; Phillips et al., 2016), on the Mid-Norwegian margin (Muñoz-Barrera et al., 2020; Osmundsen et al., 2020; Osmundsen & Péron-Pinvidic, 2018) and on the Finnmark Platform (Koehl et al., 2018). We utilise seismo-acoustic signatures in facies recognition to correlate units and discuss compositional and structural heterogeneities. Due to Cenozoic uplift in the western Barents Sea, the top of acoustic basement is located at relatively shallow levels within the study area. This improves seismic resolution and allows a detailed study of seismic basement facies and early basin evolution. Our work on deep structures of

Highlights

- Intrabasement seismic reflection analysis reveal discrete seismic facies below seismic top basement and provides evidence of Caledonian deformation and post-Caledonian detachment faulting in the central SW Barents Sea.
- Deep-seated shear zones in metamorphic basement are prone to reactivation during subsequent rift phases and exert control on structural evolution.
- Continued detachment faulting leads to successive incision, establishing interacting but subsequent detachment faults with associated exhumation of metamorphic core complexes.
- Detachment faulting and footwall uplift in the form of metamorphic core complex exhumation establishes so-called supradetachment basins.
- Isostatically induced, along-strike topographic variations along the detachment fault exerts control on supradetachment basin configuration and sedimentary distribution.

the central SW Barents Sea unravels Late Paleozoic late to post-orogenic extensional tectonics and structural inheritance in present-day structural configurations.

2 | GEOLOGICAL SETTING

The crystalline basement of the SW Barents Sea (Figure 1) corresponds to that recorded in the North Atlantic Caledonides (Braathen et al., 1999, 2018; Corfu et al., 2014; Doré, 1995; Faleide et al., 1984, 1993; Gabrielsen et al., 1990; Gac et al., 2016; Gernigon et al., 2014; Gudlaugsson et al., 1998; Johansen et al., 1993; Otto & Bailey, 1995; Ritzmann & Faleide, 2007; Serck et al., 2017; Smelror et al., 2009). The Ordovician–Early Devonian Caledonian orogen (Corfu et al., 2014) is recognised as a >2,000 km long mountain chain comprising thrust sheets attributed to contractional deformation and metamorphism throughout western Scandinavia and eastern Greenland. The Caledonian orogen is regarded as comparable in size to the modern Himalayan–Tibetan system (Corfu et al., 2014; Gudlaugsson et al., 1998) and in having significantly reworked crystalline basement. In contrast to the Caledonides elsewhere in the North Atlantic region, the nature of this orogenic belt still

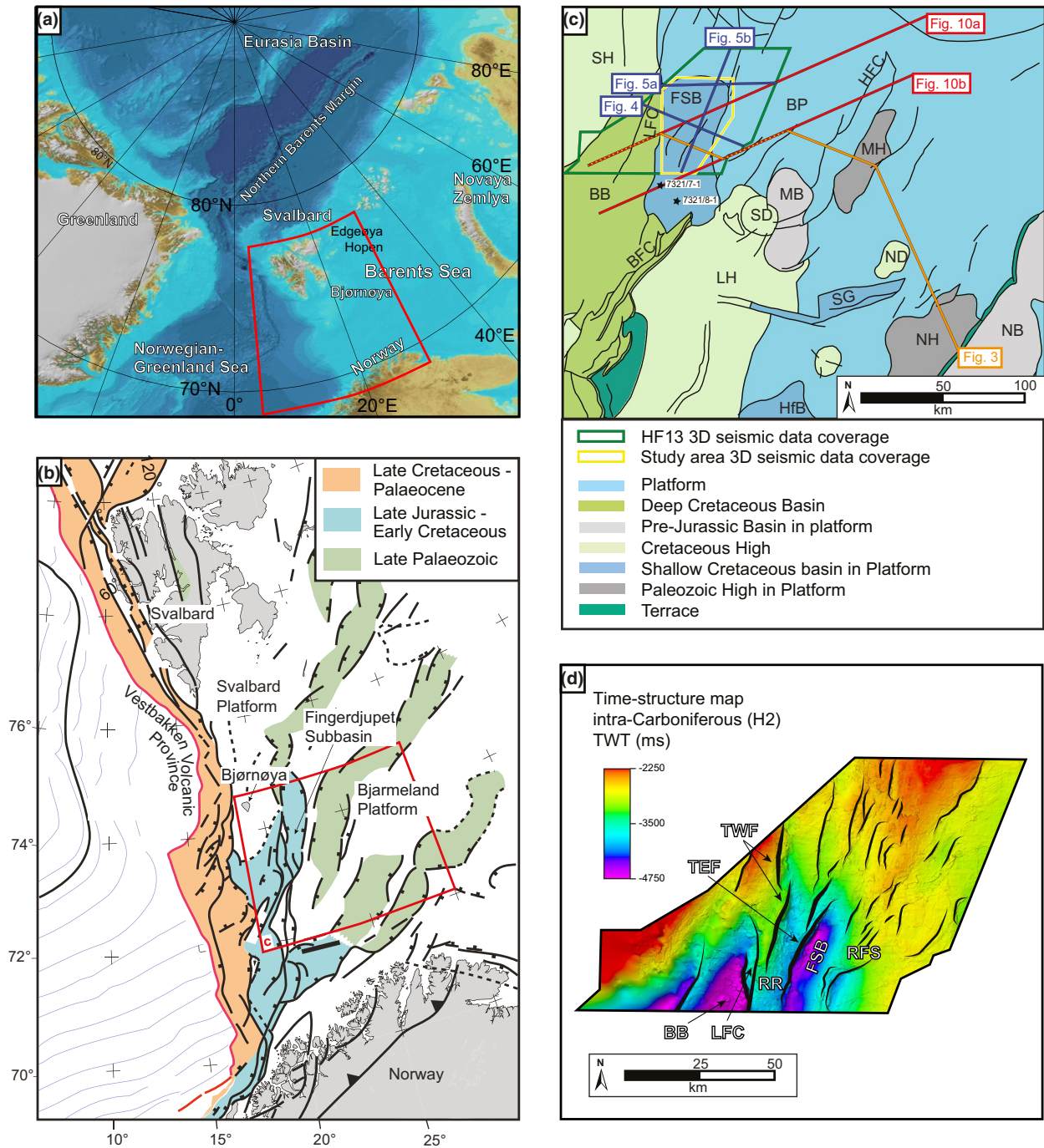


FIGURE 1 The study area is located in the southwestern Barents Sea. (a) The southwestern Barents Sea in the Arctic (modified from Jakobsson et al., 2012). (b) Structural relief of the southwestern Barents Sea (modified from Faleide et al., 2015). (c) Location of the Fingerdjupet Subbasin and adjacent areas. Structural elements are colour coded based on the period of formation and structural type of features (NPDF, 2020). Location of key seismic lines and data coverage is marked with corresponding figure annotation. (d) Time-structure map of the intra-Carboniferous reflector (H2) within the HF13 3D-seismic data cube. BB: Bjørnøya Basin; BFC: Bjørnøyrenna Fault Complex; BP: Bjarmeland Platform; FSB: Fingerdjupet Subbasin; HfB: Hammerfest Basin; HFC: Hoop Fault Complex; LFC: Leirdjupet Fault Complex; LH: Loppa High; MB: Maud Basin; MH: Mercurius High; NB: Nordkapp Basin; ND: Norvarg Dome; NH: Norsel High; RFS: Randsfjord Fault Set; RR: Ringsel Ridge; SD: Svalis Dome; SG: Swaen Graben; SH: Stappen High; TEF: Tervingen East Fault; TWF: Tervingen West Fault

remains poorly understood in the western Barents Sea and across northern Greenland to Canada (e.g. Braathen et al., 2018).

Reports of numerous Devonian extensional shear zones that reactivated former major thrusts are abundant elsewhere in the region (Braathen et al., 2002; Fossen, 2010).

Many works describe such reactivation in Southwest Norway (e.g. Braathen et al., 2004; Krabbendam & Dewey, 1998; Osmundsen & Andersen, 2001; Osmundsen et al., 2003), Central Norway (Braathen et al., 2000, 2002; Osmundsen et al., 2006; Wiest et al., 2020), the Fjord Region of East Greenland (Hartz et al., 2000) and in NW Svalbard (Braathen et al., 2018). Some of the shear zones juxtapose deeply subducted lower crustal rocks (mainly amphibolites, some granulites and locally eclogites) in a lower plate with an upper plate assemblage of Caledonian nappes and Devonian basins. In Western Norway, the kinematics of this significant unroofing event show interplay between extension and oblique-slip movements during formation of major synforms and antiforms or corrugations, parallel to upper plate tectonic transport (Braathen & Erambert, 2014; Osmundsen & Andersen, 2001). These structures form the basis for models advocating for two shortening axes and one extension axis, consistent with constrictional strain (Braathen et al., 2002; Krabbendam & Dewey, 1998; Osmundsen & Andersen, 2001; Osmundsen et al., 2003). Similarly, constrictional strain with an N–S extension axis was attributed to the Ellesmerian Orogeny linked to the Devonian Keisarhjelmen Detachment of Svalbard (Braathen et al., 2018). In the SW Barents Sea, Devonian extensional shear zones below the Late Paleozoic to recent sedimentary successions have been proposed (e.g. Gernigon & Brönnner, 2012), but their locations and importance remain unconstrained.

The SW Barents Sea region presumably comprises a highly heterogeneous crust, including strongly deformed Precambrian basement below Caledonian allochthonous units, overprinted by Devonian shear zones and buried beneath supradetachment basins (Braathen et al., 1999, 2018; Corfu et al., 2014; Faleide et al., 1984, 1993; Gabrielsen et al., 1990; Gac et al., 2016; Gernigon et al., 2014; Koehl et al., 2018; Ritzmann & Faleide, 2007; Serck et al., 2017; Smelror et al., 2009). Former analyses of seismic reflection and refraction data advocate for two Caledonian contractional belts in the SW Barents Sea: (1) a main, N–S oriented suture that stretches from the current NE Atlantic rift between Greenland and Norway to Svalbard and (2) a subordinate belt oriented NE–SW towards the Arctic (Braathen et al., 1999; Breivik et al., 2005; Gudlaugsson et al., 1998). Recent data suggest that negative, NNW–SSE oriented magnetic anomalies delineate the N–S belt. These anomalies have been interpreted as Late Paleozoic units within the SW Barents Sea region (Gernigon & Brönnner, 2012). The same data suggest that the NE–SW Caledonian arm may not exist. According to Shulgin et al. (2020), this signature reflects residual magnetism of the Timanian orogeny during Ediacaran times. The trend of magnetic signatures has been proposed as the axis of late/post-Caledonian extension, that

is approximately N–S (Gernigon & Brönnner, 2012). The magnetic signatures of the Caledonian fabric appear to be oriented at a high angle to the Late Paleozoic NE–SW horst and graben system of the western to central part of the region and essentially parallel to the N–S basins of the northwestern part of the region (e.g. Gudlaugsson et al., 1998; see also Braathen et al., 2012; Doré, 1995; Faleide et al., 1984, 1993; Gabrielsen et al., 1990; Gernigon et al., 2014; Johansen et al., 1993; Serck et al., 2017; Smelror et al., 2009). This N–S trend is also prevalent among the latest Paleozoic to Mesozoic faults in the westernmost SW Barents Sea.

Coarse-grained Devonian sediments fill intermontane basins in the Caledonian realm (Braathen et al., 2018; Osmundsen et al., 1998). They reflect deposition in fault-bound accommodation above major detachments, prior to the broad subsidence and peneplanation that occurred before the mid-Carboniferous rifting (Corfu et al., 2014; Gabrielsen et al., 1990; Smelror et al., 2009). Outcrops of Bjørnøya testify to this scenario, comprising late Proterozoic to Ordovician compressional nappes followed by extensional block faulting in the late Devonian–Mississippian, with consistent E–W tectonic transport (Braathen et al., 1999).

Outcrop studies on Svalbard and the Norwegian mainland indicate that orogenic denudation began in the Devonian to Carboniferous and was fully achieved by early Permian times (Koehl et al., 2018). However, Serck and Braathen (2019) describe Upper Permian growth sequences in the Fingerdjupet Subbasin, probably reflecting a northern continuation of Permian rifting as strongly expressed in the North Sea (Faleide et al., 2008; Fazlikhani et al., 2017). This observation substantiates the conclusions of various authors, who have identified the mid-Carboniferous to early Permian, late Permian to Early Triassic, Middle-Late Jurassic and the Early Cretaceous as periods of widespread extensional faulting affecting the SW Barents Sea (Anell et al., 2013, 2016; Braathen et al., 1999, 2018; Corfu et al., 2014; Doré, 1995; Faleide et al., 1984, 1993; Gabrielsen et al., 1990; Gac et al., 2016; Gudlaugsson et al., 1998; Johansen et al., 1993; Serck et al., 2017; Smelror et al., 2009).

2.1 | Tectonic setting of the Fingerdjupet Subbasin

The Fingerdjupet Subbasin is located in the SW Barents Sea, on the northwestern corner of the Eurasian plate (Figure 1). Following Serck et al. (2017), the basin was initially established during the Late Paleozoic as a first-order half-graben, when the Bjarmeland Platform was down-faulted to the west. Faulting was accommodated

by the listric, N–S to NNE–SSW striking Terningen Fault Complex. Repeated down-faulting along the Terningen Fault Complex developed the basin along the western flank of a major rollover monocline during the Mesozoic. Outer-arc extension and collapse of this rollover monocline in the Mesozoic explain the secondary synthetic and antithetic faults of the Randi Fault Set, which marks the eastwards extent of the Fingerdjupet Subbasin.

Several fault segments of the Terningen Fault Complex separate the Fingerdjupet Subbasin from the Ringsel Ridge. In the west, the ridge is bound by the Leirdjupet Fault Complex and the Bjørnøya Basin (Figure 1; Serck et al., 2017). The Fingerdjupet Subbasin's main depocenter is separated from the Ringsel Ridge by the NNE–SSW striking Terningen East fault. At deeper levels, dip of this fault changes significantly, from 55°–70° above top seismic basement to 5°–10° in the south and 15°–35° in the north below top seismic basement. The lower dipping segments parallel a seismic facies belt considered to represent an east-dipping detachment (Serck & Braathen, 2019). The Terningen East fault dictates the structural configuration of the southern part of the subbasin. To the north, the study area is dominated by extensional half-graben geometries where several NNE–SSW striking, east-dipping, listric faults continue into the same basement detachment (Serck & Braathen, 2019).

Four distinct periods of extensional faulting have been documented along the Terningen East fault; mid-late Carboniferous, late Permian, latest Jurassic to Hauterivian and lastly late Aptian. Suspected post-late Albian periods of extensional faulting cannot be constrained as late Cenozoic uplift caused erosion of post-upper Albian strata (Serck & Braathen, 2019; Serck et al., 2017). The study area is located near a proposed main Caledonian lineament across the SW Barents Sea (Braathen et al., 2018; Gudlaugsson et al., 1998; Ritzmann & Faleide, 2007), holding an optimal geographic position for discussing late/post-Caledonian and subsequent deformation in the region. As the Mesozoic evolution of the Fingerdjupet Subbasin is well-documented in other works, this study describes the influence and control exerted by the deep, pre-Mesozoic structural fabrics for late to post-Caledonian development.

3 | DATASETS AND METHODS

The seismic reflection data used in this study include the HF13 3D data cube which covers an area of ca. 2,800 km² down to 7 s TWT and various long-offset 2D data (Figure 1). All seismic data have been provided by TGS. We display the seismic reflection data in zero-phase and follow the Society of Exploration Geophysicists (SEG)

normal polarity convention; that is a positive reflection coefficient (downward increase in acoustic impedance) is represented by a peak (white/red) and a negative reflection coefficient (downward decrease in acoustic impedance) is represented by a trough (black). Seismic ties to hydrocarbon exploration wells near the study area were performed and correlated with previous works, for example, Serck et al. (2017). As the lowermost stratigraphic sequence drilled in close proximity to the study area is Upper Permian in age (Wellbore 7321/8-1; NPDF, 2020), we tentatively date older sequences based on seismic signature combined with stratigraphic position and further correlate with interpretations from Hassaan et al. (2019) (Figure 2).

The offshore aeromagnetic data used in this study are from a compilation of the BASAR09 project of the Geological Survey of Norway (NGU) published by Gernigon and Brønner (2012) and Gernigon et al. (2014). Magnetic properties from well core measurements generally show low susceptibilities, suggesting that deeper-lying basement bodies with high susceptibilities and/or remnant magnetisation cause the anomalies (Gernigon & Brønner, 2012).

Our approach uses intra-basement seismic reflectivity derived from lithological changes, which create noticeable interfaces, and to a lesser degree interference and/or scattering effects. It is noted that lack of well control within basement introduces uncertainty in basement seismic facies interpretation. We presume that reflectivity may indicate metamorphic modifications by ductile deformation, readily identified in major, low-angle shear zones or detachments (Braathen et al., 2004). Many authors have proposed such low-angle detachments in the North Sea, the Mid-Norwegian margin and in rifted margins elsewhere (e.g. Fazlikhani et al., 2017; Fossen, 2010; Koehl et al., 2018; Lenhart et al., 2019; Osmundsen & Ebbing, 2008; Phillips et al., 2016). Following these studies, characterising distinct seismic facies requires that the facies has a (1) distinguishable geometric shape, with (2) distinguishable internal trend and reflection characteristics, which are (3) recognisable over larger areas. To rule out seismic artifacts and assess whether the observed basement reflectivity is authentic, the data were inspected for possible multiples, diffraction and migration artifacts.

The stratigraphic position and geometrical constraints of the different seismic facies and the relationships between them were investigated to determine whether the facies were bound by faults and/or distinct or transitional changes in reflection patterns. Along with fault interpretation, five seismic horizons (H1-5) and five sedimentary sequences (S1-5) above top-basement were mapped and dated based on seismic-to-well-ties from wells 7321/7-1, 7321/8-1, 7229/11-1 and 7130/4-1

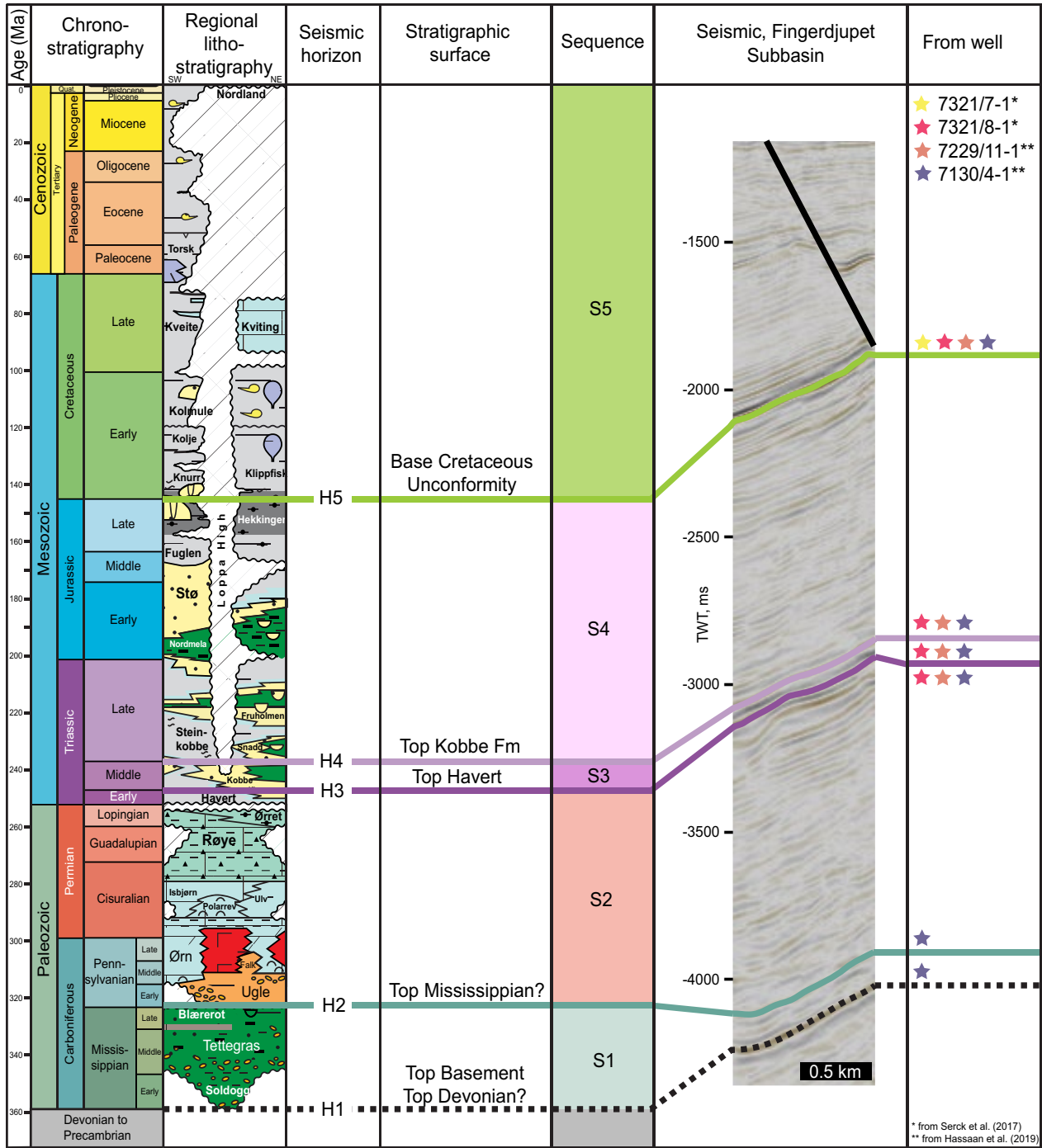


FIGURE 2 Stratigraphic framework within the Fingerdjupet Subbasin, based on well correlations, correlated with Serck et al. (2017) and Hassaan et al. (2019). Seismic sequence from 3D seismic composite in Figure 4, see Figure 1 for location. Chronostratigraphic and regional lithostratigraphic chart modified from Gradstein et al. (2012). Seismic data courtesy of TGS

(Figure 2; i.e. Serck et al., 2017; Hassaan et al., 2019). The H1 reflector is defined as top acoustic basement, marking the transition from sedimentary sequences to basement units. The H2–H5 horizons were mapped primarily to establish stratigraphic control above the Top Basement reflector and are therefore not further elaborated upon. Four distinct intrabasement seismic facies

units (SF1-4) were mapped according to the criteria as listed above. Time-structure and -thickness maps were generated for two intra-basement seismic facies boundaries: HB1 and HB2. The results of the detailed seismic facies analysis performed within the 3D dataset were tied to interpretations of regional 2D lines and correlated with potential field data.

4 | RESULTS

Figure 3 illustrates how Paleozoic to Mesozoic strata within the Fingerdjupet Subbasin are involved in the mentioned rollover mostly facilitated by the Terningen Fault Complex. The Terningen Fault Complex soles out in an east-dipping detachment at depth and exhibits a listric geometry which is preserved also in depth-converted seismic sections (Serck et al., 2017). Inferred Pennsylvanian deposits display a wedge-shape thickening towards the Terningen Fault Complex and retain a tabular geometry eastward. Similar-age deposits thicken towards steep faults bounding half-graben basins such as the Maud and Ottar basins east and southeast of the study area, respectively. As described in Hassaan et al. (2019) and Larssen et al. (2005), these Late Paleozoic basins include a Carboniferous package assumed to be of Mississippian age, not identified within the Fingerdjupet Subbasin.

4.1 | Intrabasement seismic facies

Starting in the west, sedimentary strata and interpreted intrabasement horizons show displacement along major faults in the Terningen Fault Complex, which we refer to as the Terningen East fault and Terningen West fault (after Serck et al., 2017) (Figure 4). We identify four seismic facies below Top Basement, represented by the H1 reflector. Uninterpreted seismic sections corresponding to those presented in Figures 4 and 5 are available in supplementary material.

Seismic Facies 1a (Figure 4; SF1a) is characterised by low amplitude, semi-transparent, semi- to discontinuous, cross-cutting reflections, locally subparallel to the overlying H1. The low amplitude reflections within SF1a are

deemed a result of lacking velocity/density variations, pointing towards relatively homogeneous facies. Thin, sequenced layering may still be present, masked by the seismic limit of visibility. As no indications of tuning effects are identified, this would apply for the entire vertical extent of SF1a. SF1a is traceable throughout the study area, forming a trough-like geometry (Figure 5a). This facies signature coupled with geometry, and a position at the top of the basement, suggests that SF1a represents sedimentary units, consistent with Devonian (meta-)sedimentary units as described elsewhere (see Discussion).

Seismic Facies 1b (Figure 4; SF1b) consists of relatively continuous, sub-parallel, gently W-dipping, low to moderate amplitude reflections in the upper part of the basement. SF1b is bound by SF3 and H1 and occurs above Seismic Facies 2 (SF2) in the western parts of the study area (Figures 4 and 5a). An angular unconformity is proposed for H1, as it truncates top-lapping reflectors. SF2 is identifiable in the entire study area, with varying lateral thickness and westward thickening wedge-shaped packages against faults. The internal reflectivity of SF1b resembles that of SF1a; however, differences include geometrical extent and bounding facies (i.e. wedge-shaped packages overlying SF2). SF1b presumably constitutes Devonian metasediments in the uppermost part of seismic basement.

SF2 (Figure 4; SF2), the upwards extent of which is mapped as HB2, is best expressed in western part of the study area, showing lower amplitudes in the northeast. This facies consists of moderate- to high-amplitude, semi-continuous, sub-parallel, mostly SE-dipping and occasionally curved reflections, in stark contrast to the more transparent SF1a and SF1b. Notably, some reflections that cross-cut the overall SE-dipping reflections are identified as unsuppressed multiples. SF2 is offset by large faults aligning with internal reflectors. Based on its crustal position,

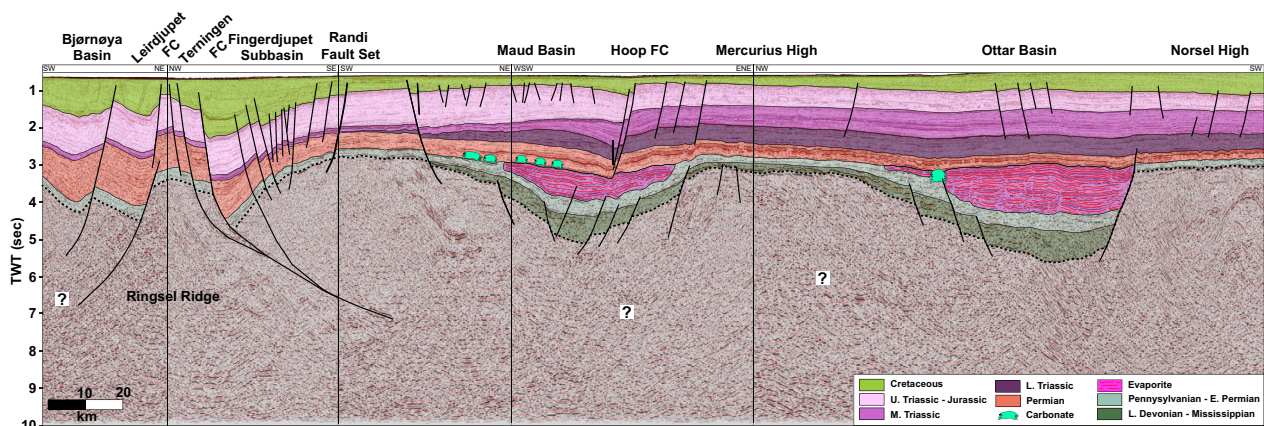
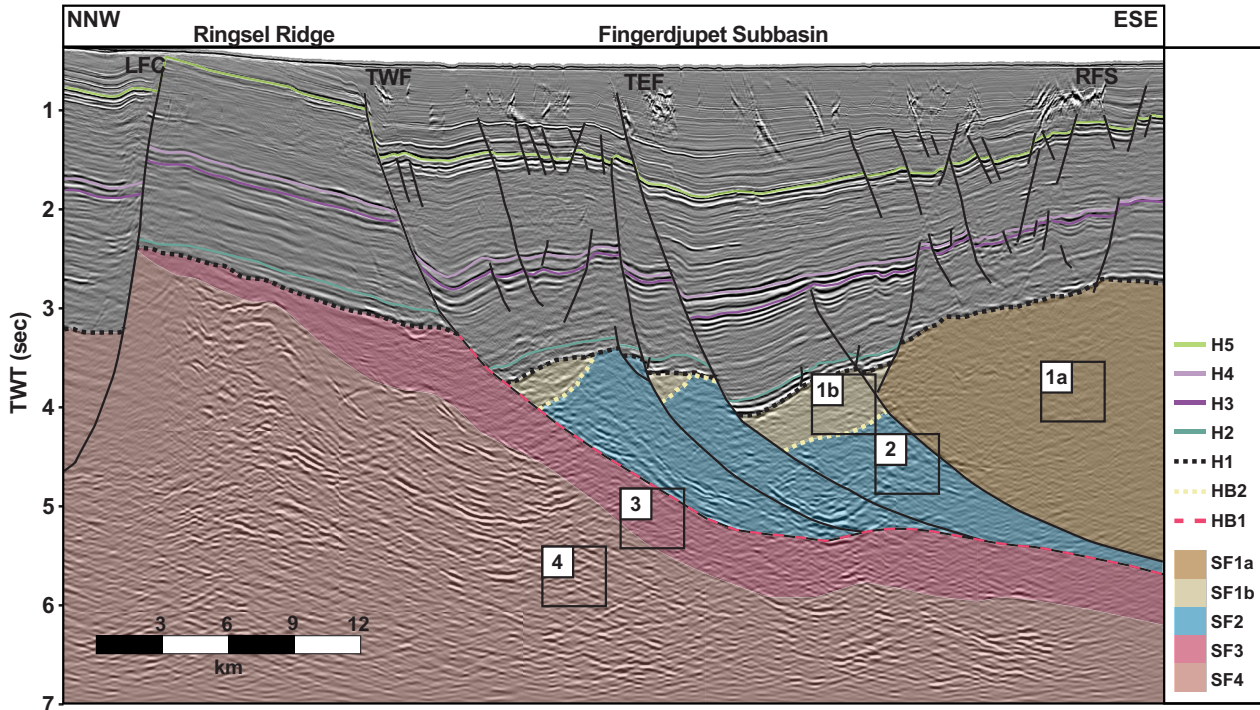
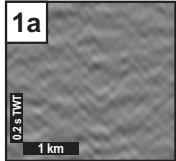


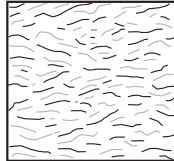
FIGURE 3 2D seismic regional composite, see Figure 1 for location, from the Bjørnøya Basin to the Norsel High. Late Paleozoic and Mesozoic strata are downfaulted against the listric Terningen Fault Complex, separating the Fingerdjupet Subbasin from the Ringsel Ridge. The Maud and Ottar basins hold Mississippian and evaporite deposits which are not present in the Fingerdjupet Subbasin. Stippled line marks top basement/Top Devonian? Seismic data courtesy of TGS



Seismic



Line drawing

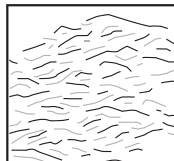
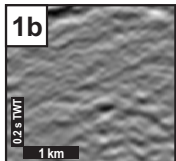


Key observations

- Low amplitude, chaotic, semi-transparent, semi- to non-continuous reflections
- Saucer shaped geometry

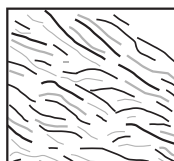
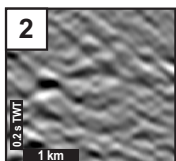
Interpretation

Devonian metasedimentary units



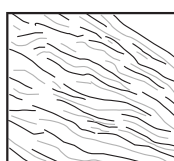
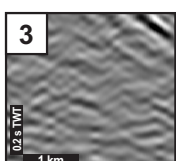
- Low to moderate amplitude, chaotic, semi-transparent, semi-continuous reflections
- Wedge-shaped with varying lateral thickness

Devonian metasedimentary units



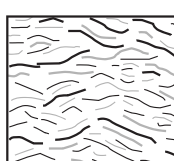
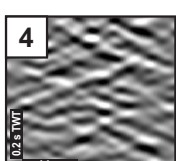
- Moderate to high amplitude, semi-continuous, sub-parallel, occasionally folded reflections.
- SE-dipping package with SE-dipping reflections

Allochthonous units



- Semi-parallel, medium amplitude reflections with high frequency and medium continuity
- Package dips SE with SE-dipping reflections in the south, bends concave upward in the north

Shear zone



- Discontinuous, cross-cutting, moderate to locally very high amplitude reflections of varying orientation
- Largest accumulations in domal structures in W and E joined by E-W striking anticline

Autochthonous basement

FIGURE 4 3D seismic composite, see Figure 1 for location. Late Paleozoic and Mesozoic strata are downfaulted against the listric Terningen Fault Complex (TWF and TEF), separating the Fingerdjupet Subbasin from the Ringsel Ridge. Below the H1 reflector, intrabasement seismic facies interpretations are colour coded based on outlined characteristics. Boxes mark locations of zoomed seismic sections of each respective seismic facies SF1a-4. TEF records the most displacement, but Late Paleozoic to Mesozoic strata are also displaced along the TWF, both faults displace intrabasement seismic facies unit SF2, and SF1b thickens towards the same faults. All faults sole out onto the HB1 reflector. LFC: Leirdjupet Fault Complex; TEF: Terningen East Fault; TWF: Terningen West Fault; RFS: Randi Fault Set. Seismic data courtesy of TGS

geometry, reflectivity and both the external and internal shapes (i.e. high-dip reflections, wedge-shaped geometry), we interpret SF2 as Caledonian allochthonous nappes.

Seismic Facies 3 (Figure 4; SF3) has semi-parallel, medium amplitude to semitransparent reflections with high frequency and medium continuity and is bound by high-amplitude reflections. In the NE, the internal reflectivity of SF3 becomes more chaotic. Reflection sets form 200–400 ms TWT thick packages, dipping SE-wards in the southern part of the study area. Below 5 s TWT, the boundaries of SF3 undulate and the internal reflection pattern shift from (semi-) parallel to more chaotic and cross-cutting, dominated by anastomosing geometries (Figure 5). The western limitation of SF3 lies within the Ringsel Ridge, where the facies is truncated by the H1 reflector (Figure 4), while the eastern limit lie beyond the 3D dataset. In the northeast, SF3 has a convex upwards geometry and forms an E–W trending antiformal culmination (Figure 5). SF3 is capped by the downward continuation of the Terningen East fault, represented by a high amplitude, locally continuous reflection. We interpreted this to represent the detachment fault surface, denoted as HB1. The other faults in the Terningen Fault Complex terminate onto HB1 or in SF3 (Figures 4 and 5). Fault terminations, the internal reflectivity, alternating geometrical shape and extent at depth suggest that SF3 is a shear zone.

Seismic Facies 4 (Figure 4; SF4) consists of discontinuous, moderate to very high-amplitude reflections of varying orientations, comprising changing geometries. There is a transitional shift from the semi-parallel, moderate-amplitude reflections within SF3 to the stronger, more chaotic reflections of SF4. This pattern is found in the outer and deeper parts of the study area, where it mainly appears below SF3 but reaches the H1 reflector in the Ringsel Ridge. SF4 extends to the lower limit of the data set at 7 s TWT. In the eastern and western parts of the study area, SF4 has greater TWT thickness and reaches shallower levels forming large antiformal culminations (Figure 5). Based on its characteristics and crustal position, we interpret SF4 as pre-Caledonian basement. SF4 antiforms presumably reflect extensive footwall uplift involving upwelling of crustal material (in a core complex; see Discussion) due to major extensional movements as indicated by the interpretations of SF1-3.

4.2 | Correlation with magnetic anomaly response

Figure 6 shows the tilt-derivate filtered magnetic anomaly map, presented by Gernigon and Bröner (2012), time-structure maps for intrabasement horizons HB1 and HB2 and a time-thickness map between HB2 and H1, corresponding to the vertical distribution of SF1a-b. The three key positive magnetic anomalies for this study are denoted as MA1, MA2 and MA3.

MA1 coincides with the spatial extent of the Ringsel Ridge and outlines the western boundary of the Fingerdjupet Subbasin. As the Ringsel Ridge constitutes facies SF4 (Figures 4 and 5) partly overlain by SF3, the encountered magnetic response appears interlinked with these facies belts; that is crustal rocks modified in an overlying shear zone. MA2, on the other hand, correlates with an increased vertical distribution of facies SF2 (Figure 6d). MA2 also partly coincides with the E–W trending antiformal dome of HB1 which, following the interpretations above, represents the top shear zone SF3 and detachment fault surface (Figure 6). In the northeast, MA3 covers a second domal structure consisting mainly of SF4, capped by two wedges of SF2 (Figure 5a). Higher velocities within SF2 may facilitate seismic pull-up and cause seismic artifacts. However, the maximum accumulations of SF2 do not correlate with the stratigraphic highest levels of SF3-4. On the contrary, MA3 is larger than MA2, and the vertical thickness of SF2 is lower above MA3 relative to MA2 (Figure 5a). MA2 overlaps geographically with both the distribution of SF2 and the antiformal geometry (Figure 6b–d). The vertical distribution of SF1a-b (Figure 6e) correlates roughly to low magnetic anomaly values (Figure 6b).

Our interpretations in Figures 4 and 5, combined with the correlation between seismic and potential field data (Figure 6), form the basis for the schematic 3D illustration of the area presented in Figure 7. Sedimentary units of Devonian age (SF1a–SF1b) overlie allochthonous units (SF2) separated by HB2. HB1 separates SF3 from SF2 and is interpreted to correspond to a major detachment fault, the Fingerdjupet detachment. SF2-4 constitutes a concave upwards, E–W trending antiform in the central part of the subbasin, which in the easternmost part of the study area

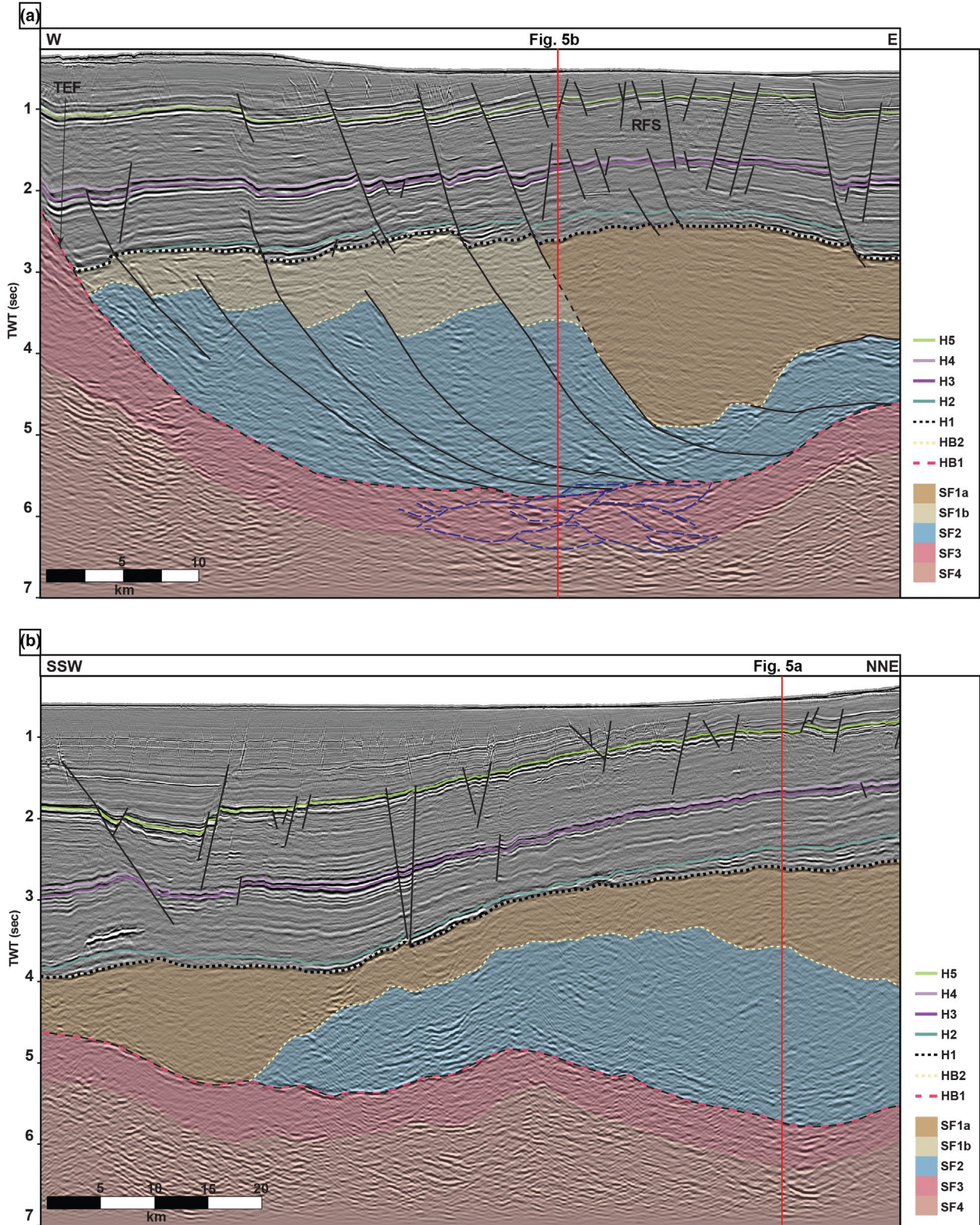


FIGURE 5 (a) 3D seismic composite line, see Figure 1 for location. Below the H1 reflector, intrabasement seismic facies interpretations are colour coded based on outlined characteristics. SF3 attains an upwards concave geometry to the east, capped by to highly rotated units of SF2. SF4 and SF3 climb to shallower levels both to the west and east, the former notably to higher levels than the latter. All faults sole out onto the HB1 reflector. Blue stippled lines mark interpretations of anastomosing geometries within SF3. Red line indicates intersection of Figure 5b. (b) 3D seismic composite line, see Figure 1 for location. SF3 shows an anticlinal geometry, closely corresponding to an increased accumulation of SF2. Red line indicates intersection of Figure 5a. RFS: Randi Fault Set; TEF: Terningen East Fault. Seismic data courtesy of TGS

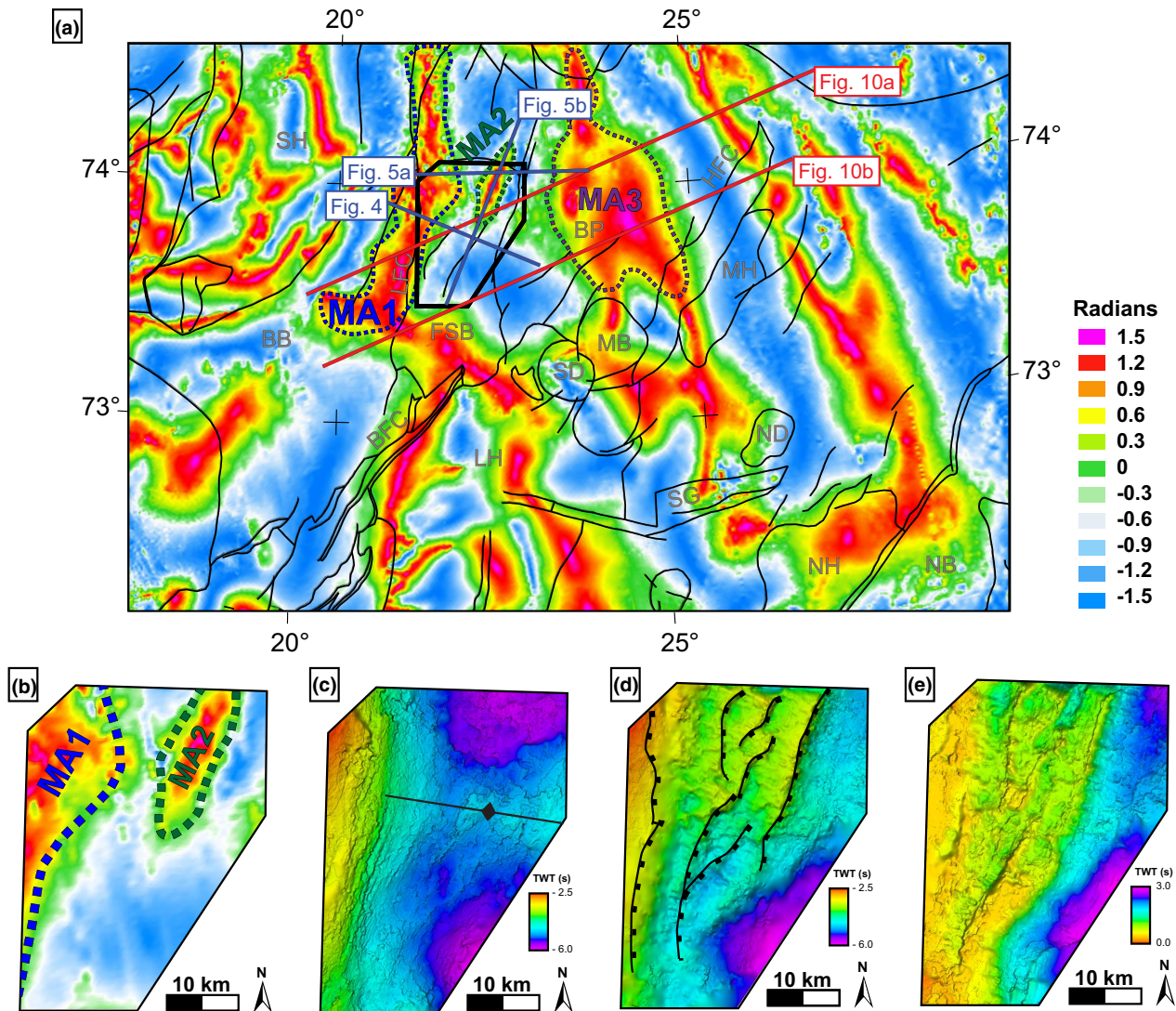


FIGURE 6 (a) Tilt derivate filtered magnetic anomaly map, as presented by Gernigon and Brønner (2012) and Gernigon et al. (2014). Red and blue lines indicate locations of key 2D seismic and composite 3D seismic lines, respectively. Black polygon indicates location of study area and extent of enlarged sections in b–e. MA1–3 outlines main magnetic anomalies adjacent to the study area. (b) Enlarged tilt derivate filtered magnetic anomaly map for study area. (c) Time-structure map of intrabasement seismic horizon HB1, corresponding to the downwards continuation of the Terningen Fault Complex. Note the distinct E–W trending antiformal geometry. (d) Time-structure map of intrabasement seismic horizon HB2 (Top SF2) with location of basement displacing normal faults, all with downthrow to the east. (e) Time thickness isochore map between horizons HB2 and H1, corresponding to the distribution of SF1a–b. BB: Bjørnøya Basin; BFC: Bjørnøyrenna Fault Complex; BP: Bjarmeland Platform; FSB: Fingerdjupet Subbasin; HfB: Hammerfest Basin; HFC: Hoop Fault Complex; LFC: Leirdjupet Fault Complex; LH: Loppa High; MB: Maud Basin; MH: Mercurius High; NB: Nordkapp Basin; ND: Norvarg Dome; NH: Norsel High; SD: Svalis Dome; SG: Swaen Graben; SH: Stappen High. Magnetic anomaly data courtesy of NGU

culminates in highly rotated units of SF2 overlying SF3–4. Upwelling of SF4 is interpreted to have occurred beneath both the Ringsel Ridge and again to the east. We attribute these vertical crustal movements to large-scale displacement along two detachment faults; the Fingerdjupet detachment and a second detachment fault further east (Figure 7).

5 | DISCUSSION

5.1 | Seismic facies in the basement

In the below discussion, we review the proposed seismic facies in the light of seismic resolution, onshore-offshore correlations, and structural and depositional models.

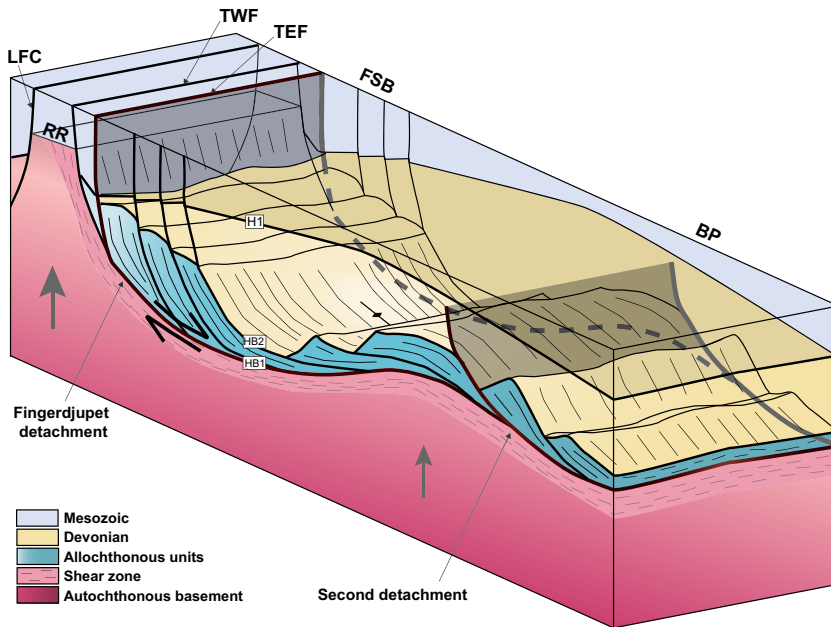


FIGURE 7 Conceptual illustration of the proposed structural configuration within the Fingerdjupet Subbasin. Upwelled crustal material is indicated with grey arrows. Not to scale. BP: Bjarmeland Platform; FSB: Fingerdjupet Subbasin; LFC: Leirdjupet Fault Complex; RR: Ringsel Ridge; TEF: Terningen East Fault; TWF: Terningen West Fault

We aim to substantiate their tectonostratigraphic significance through discussions of regional and conceptual frameworks.

5.1.1 | SF1a

Facies SF1a resembles the Devonian metasediments as interpreted in offshore-onshore correlation works from Svalbard (Bælum & Braathen, 2012; Bergh et al., 1997) and in conventional seismic interpretations on the Finnmark Platform (Koehl et al., 2018). The apparent lack of reflectivity may be attributed to relatively homogeneous sediments without major important velocity/density contrasts across the bedding. This may be expected in anchizone (sub)metamorphic sediments with no or very little preserved primary porosity, such as reported from the Lower to Middle Devonian sediments preserved onshore Norway (e.g. Souche et al., 2012). The transparent characteristics of the facies neither constrain nor exclude folds and tilted geometries as described in Devonian strata on Svalbard (Braathen et al., 2018) and onshore Norway (Osmundsen et al., 2006). Despite the lack of internal identification, the folded substrate geometry (HB2: Figure 6c) indicates the presence of such structures. This would, however, require that the structural configuration of HB2 was syn- or post-depositional, which remains an unconstrained scenario.

5.1.2 | SF1b

We differentiate SF1b from SF1a based on tectonostratigraphic position and different bounding facies. Interpreting SF1b as Devonian sedimentary units

implies deposition of SF1b within wedge-shaped, nappe constrained basins formed through extensional reactivation and back-sliding or fault dissection. Outcrop studies on Bjørnøya support these observations (Braathen et al., 1999). Supradetachment basins have been proposed to be dominated by footwall-derived transverse drainage networks due to high uplift rates and footwall erosion (Friedmann & Burbank, 1995; Serck et al., 2021). This would entail erosion of both the Ringsel Ridge and SF2. However, isostatic rebound may cause basin inversion and drainage divide in areas of maximum extension (Kapp et al., 2008). The erosion and deposition of Devonian sediments would then be concentrated to the north and south of SF2, explaining the preservation of SF2 and the lateral variability between SF1a and SF1b (Figure 6e). Following the estimates of e.g. Hedin et al. (2016) for basement velocities of 6 km/s entails a thickness of the Devonian metasedimentary strata of roughly 9 km in the deepest parts of the Fingerdjupet Subbasin (Figure 6e). These values are within the range of reported Devonian basin fill thicknesses from field work studies in e.g. the Billefjorden Trough (>6 km) on Svalbard (Braathen et al., 2018) and the Devonian basins of western Norway (>26 km) (e.g. Vetti & Fossen, 2012).

5.1.3 | SF2

Facies SF2 shows large internal amplitude variations in the 3D seismic dataset and is interpreted as strongly deformed material similar to the interpretations of Lenhart et al. (2019) from the northern North Sea. SE-dipping reflections within SF2 indicate an E to SE tectonic transport direction. The Stappen High has been suggested to

represent the western margin of a westerly directed thrust during the Caledonian orogen experiencing significant footwall uplift (Braathen et al., 1999). The location of the Fingerdjupet Subbasin east of the Stappen High implies westward thrusting also within the subbasin, which coincides with the internal reflectivity of SF2. The SF2 deformed seismic signature advocates for the facies taking part in Early Caledonian or even older deformation. Extensional reactivation of thrust faults between Caledonian nappes explains the lateral variability of SF2 in the proximity of basin-bounding faults, similar to reports from elsewhere in the SW Barents Sea region (Braathen et al., 1999, 2018) and onshore central and western Norway (Fossen, 2010; Osmundsen et al., 2003). This supports the interpretation of SF2 as highly deformed allochthonous nappe units.

5.1.4 | SF3

Shear zones typically show parallel, high-frequency, low-amplitude reflections if the seismic resolution is high enough (e.g. Fazlikhani et al., 2017; Lenhart et al., 2019; Phillips et al., 2016; Wang et al., 1989), similar to the observed reflectivity within SF3. Similar descriptions of seismic facies interpreted as shear zones have been confirmed independently via other means, e.g. borehole data (Hedin et al., 2016) and outcrop projections (Wang et al., 1989). We identified additional characteristics for basement shear zones, that is internal reflections capped by the downwards continuation of the Terningen Fault Complex and all deep faults sole out onto SF3 (e.g. Fossen & Cavalcante, 2017). Further, ca. 2 km Cenozoic uplift combined with depth-stretching estimates places the linkage of the Terningen East fault and the Fingerdjupet detachment close to the brittle-ductile transition in the crust (ca. 12 km) (Baig et al., 2016; Fossen & Cavalcante, 2017; Serck & Braathen, 2019). Top to the east displacement along basin-bounding faults that sole out onto SF3 indicate a WNW–ESE to NW–SE strain axis.

5.1.5 | SF4

Pre-Devonian basement has been described from outcrops on Svalbard (e.g. Bælum & Braathen, 2012; Bergh et al., 1997) and Bjørnøya (Braathen et al., 1999) as non-continuous, chaotic, high amplitude reflections on offshore-onshore correlated seismic sections (e.g. Bælum & Braathen, 2012). Bergh et al. (1997) documented the heterogeneous nature of pre-Devonian basement, where deformation intensity and style display rapid lateral and vertical variations. The internal impedance contrasts within SF4 presumably reflect heterogeneous autochthonous

basement due to varying degrees of deformation. Other works have previously correlated high magnetic anomaly responses to metamorphic core complexes (e.g. Lenhart et al., 2019; Muñoz-Barrera et al., 2020). The lowermost position of the facies, combined with the internal observations and associated magnetic anomalies, suggests that SF4 features metamorphic basement and core complexes represented by antiformal culminations (Figure 6).

5.2 | Deep configuration of the Fingerdjupet Subbasin

Based on concepts outlined in Whitney et al. (2013), we suggest that extensional reactivation of rheologically weak Caledonian thrust faults resulted in the initiation of the Fingerdjupet Subbasin in the Middle Paleozoic. This is consistent with observations from Bjørnøya where Caledonian thrust faults were extensionally reactivated until late Carboniferous times (Braathen et al., 1999). Our seismic facies analysis indicates a core complex scenario, driven by lithospheric thinning. The interpreted extensional shear zone (SF3) is capped by the Fingerdjupet detachment.

Flat-lying extensional detachment zones created through the forward sequential development of steeply dipping normal faults are generally considered in terms of a rolling hinge model. This model describes how increasing extension and isostatic rebound in response to tectonic unloading rotates each new fault to a lower dip, leading to the abandonment of the low-angle fault as new faults develop in the hanging wall (Braathen & Osmundsen, 2020; Brun et al., 2018; Lister & Davis, 1989; Osmundsen & Péron-Pinvidic, 2018; Whitney et al., 2013). The east-dipping Fingerdjupet detachment parallels the N–S to NNE–SSW striking Ringsel Ridge as identified in both seismic and potential field data (MA1) (Figures 4, 5 and 7). Carboniferous growth sequences along the easternmost faults within the Terningen Fault Complex (Figure 3) testify to progressive eastward rift development during the Late Paleozoic. Footwall isostatic uplift and flexure elevated the Ringsel Ridge as an antiform normal to the extension axis, leading to shear zone truncation as described in rolling hinge models (Brun et al., 2018; Platt et al., 2015; Whitney et al., 2013). Extension calculations along seismic sections (e.g. Figures 4 and 5a) indicate that the current distribution of SF2 reflects minimum 22–31 km extension within the study area. This is consistent with previously published numerical models that were able to produce subhorizontal detachments using a rolling hinge model with ca. 27 km displacement (Lavie et al., 1999). We propose that the Ringsel Ridge represents an exhumed core complex due to the sequential extensional development of the Terningen Fault Complex. The

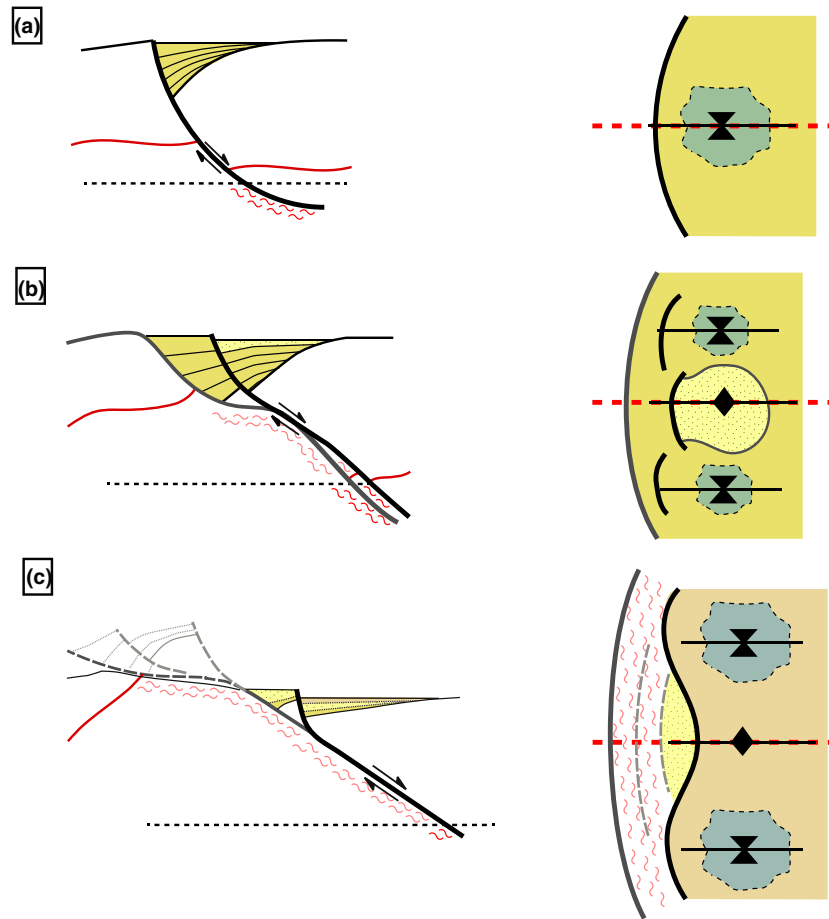


FIGURE 8 Schematic cross-sections (left) and map view (right) illustration of how isostatic uplift due to continued extensional movement may evolve during progressive a–c extension. (a) Initial faulting creates a half-graben basin with a depocenter (syncline) in area of most extension. (b) Abandonment of initial fault as a new incising fault initiates. Due to isostatic rebound in the area of maximum extension and the most crustal thinning, the detachment experiences progressive upwarping, leading to an anticline in the area of most extension. In map view, this causes drainage to reroute into newly formed synclinal depocenters. (c) Progressive extension and footwall uplift exhumes the mylonitic front and abandoned breakaway faults, separated from the formed supradetachment basin by the youngest detachment fault. Redrawn and modified from Kapp et al. (2008)

fault complex was in turn controlled by the Fingerdjupet detachment, *sensu* the rolling hinge model.

The E–W striking antiform geometry of the Fingerdjupet detachment, which partially corresponds to MA2 (Figure 6), cannot be fully explained by the rolling hinge model. Detachment faults with undulating fault surfaces, reflecting transport-parallel corrugations, have been reported from extensional systems world-wide, e.g. the United States (Holm et al., 1994; Lister & Davis, 1989; Miller & Pavlis, 2005; Seiler et al., 2013); southwest Norway (e.g. Braathen & Erambert, 2014; Chauvet & Séranne, 1994; Krabbendam & Dewey, 1998; Osmundsen et al., 1998); Tibet (Kapp et al., 2008); Papua New Guinea (Little et al., 2011); East Greenland (Hartz et al., 2000); and on Svalbard (Braathen et al., 2018). Observations from these regions in many ways appear similar; however, the suggested origins for extension-parallel folds in detachment systems vary. Orthogonal shortening and resulting extension-parallel

folds have been attributed to constrictional strains (Braathen & Erambert, 2014; Braathen et al., 2018; Holm et al., 1994), in turn attributed to regional transtension (Fossen et al., 2013; Krabbendam & Dewey, 1998; Osmundsen & Andersen, 2001). Alternatively, Kapp et al. (2008) suggested that crustal-scale fault growth may result in synclinal depocenters on either side of an antiformal core complex due to isostatic rebound, in a configuration that resembles extension-parallel folding (Figure 8).

In terms of constrictional strain, N–S shortening during the Late Paleozoic has not been documented within near our study area. Gernigon et al. (2014) proposed E–W movements along a candidate shear zone just south of the Fingerdjupet Subbasin (North of Loppa Shear Zone) based on potential field data analysis, but this remains poorly constrained. A constrictional strain field is not in accordance with our interpretation of the N–S elongated Ringsel Ridge. In the combination of the Ringsel Ridge and the E–W trending antiform

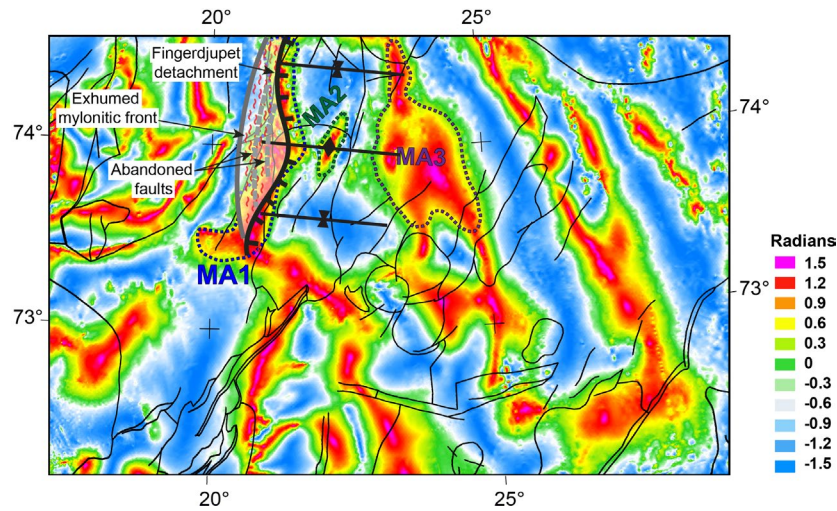


FIGURE 9 Tilt derivate filtered magnetic anomaly map, as presented by Gernigon and Brönnner (2012) and Gernigon et al. (2014). Superimposed on the map is the location of the N–S oriented Fingerdjupet Detachment with an antiformal corrugation in the area of maximum displacement, corresponding roughly to MA2. To the north and south of MA2, two synclinal depocenters are indicated, sensu Kapp et al. (2008). Magnetic anomaly data courtesy of NGU

under the Fingerdjupet Subbasin, we do, however, recognise a strong resemblance with the model of Kapp et al. (2008, see also Osmundsen & Péron-Pinvidic, 2018) (Figure 8). This is consistent with the magnetic anomalies adjacent the Fingerdjupet Subbasin (Figure 9). We propose that detachment arching due to isostatic rebound in the northern part of the study area generated an intrabasinal high, leading to two main depocenters. In this scenario, the depocenters to the N and S would hold substantial amounts of Devonian sediments (SF1a–b) separated by an intrabasinal high consisting of upwelled ductile material (SF2–4). When superimposing this model on the tilt derivate magnetic anomaly map for the area, we observe a strong correlation between the magnetic anomalies and the seismic facies. SF1a–b yields low, and SF2–4 high magnetic anomaly responses (Figure 9). It is noted that in transtensional systems, early extension-parallel folds produced by fault growth may be amplified by orthogonal shortening (Osmundsen et al., 2021). However, as the Late Paleozoic kinematic pattern in the central SW Barents Sea remains unresolved, possible additional effects of constriction due to transtensional strain cannot be addressed at this point.

5.3 | Regional implications

Following the Fingerdjupet detachment towards the Bjarmeland Platform, a second antiformal structure (SF3–4) is observed (Figure 5). The extensively rotated allochthonous units (SF2) indicate exhumation of a second core complex. We suggest that during Late Devonian large-scale extension, the Fingerdjupet detachment was rotated to subhorizontal levels during increasing displacement, encouraging the establishment of a second crustal-tapering

detachment fault, as indicated in Figure 7. Associated vertical ductile material influx established a second metamorphic core complex recording less exhumation than the Ringsel Ridge. We propose that the Fingerdjupet Subbasin overlies a ‘tectonic keel’ (sensu Reynolds & Lister, 1990) in the form of a post-orogenic supradetachment basin which experienced subsidence during Devonian deposition. The 2D and 3D data used for this study differ in terms of recording length, acquisition and processing parameters. Our interpretations below H1, east of the red line are speculative, as the line marks end of facies constraints from the 3D dataset and the 2D lines have less resolution at depth. When extrapolating the interpretations from 3D seismic data and integrating them with intrabasement reflections visible on regional 2D lines, the presence of the second detachment is indicated (Figure 10). The outlined scenario resembles the tectonostratigraphic development described for the Gossa High area in the Slørebøtn Subbasin on the mid-Norwegian margin (Osmundsen & Péron-Pinvidic, 2018).

According to models for successive development and abandonment of detachment faults (Braathen & Osmundsen, 2020; Brun et al., 2018; Osmundsen & Péron-Pinvidic, 2018; Whitney et al., 2013), the second detachment is a better candidate for continued reactivation. However, while the Terningen East fault links up with the Fingerdjupet detachment close to the brittle-ductile transition, the second detachment resides at lower crustal levels (Figure 10). The second detachment may have become inactive in the Late Paleozoic during the onset of crustal thinning and basement faulting in the western Barents Sea (e.g. Bjørnøyrenna and Leirdjupet fault complexes) (Faleide et al., 2008; Gabrielsen

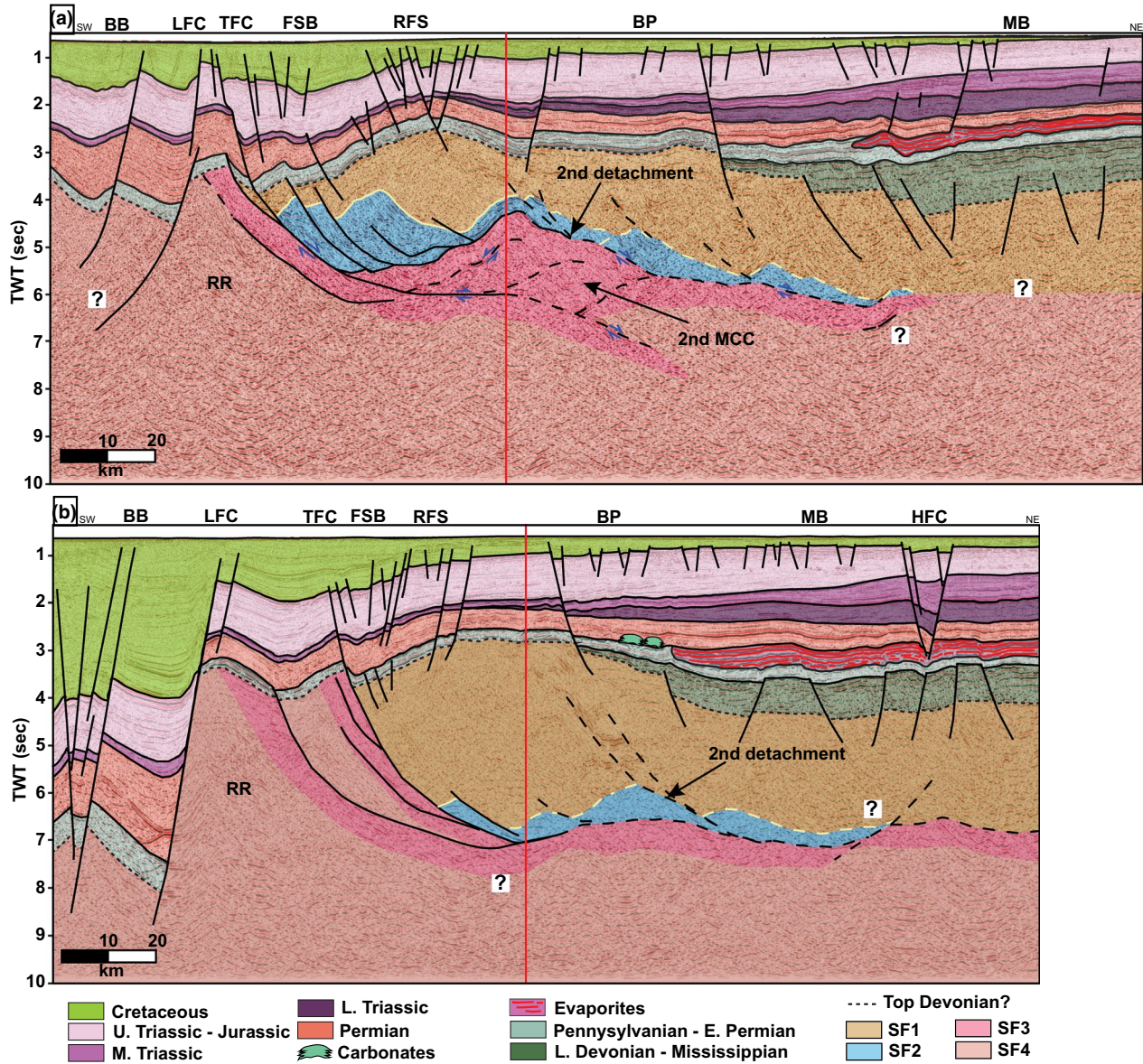


FIGURE 10 Below the H1 reflector, intrabasement seismic facies interpretations are colour coded based on interpretations within the 3D seismic data left of the red line. Right of the red line, intrabasement facies interpretations are tentative. (a) 2D seismic line, see Figure 1 for location. Below the RFS, the downwards continuation of the TFC attains a concave upwards geometry and outlines a large basement culmination, separated from SF4 by zones of strong reflectivity interpreted as SF2. This is interpreted to represent a second metamorphic core complex (MCC) to the RR. A second detachment is proposed beneath the Bjarmeland Platform, although this is, as indicated in stippled lines, a conceptual interpretation not well constrained based on seismic reflectivity. (b) 2D seismic line is located further south, see Figure 1 for location. Accumulations of SF1 are large, and SF3 is suggested in two separate zones within the RR. Distribution of SF2 is low, relative to as observed in (a), but its presence is indicated below the RFS. A second detachment is proposed also in this section, below the BP. BB: Bjørnøya Basin; BP: Bjarmeland Platform; FSB: Fingerdjupet Subbasin; HFC: Hoop Fault Complex; LFC: Leirdjupet Fault Complex; MB: Maud Basin; RFS: Randi Fault Set; RR: Ringsel Ridge; TFC: Terningen Fault Complex. Seismic data courtesy of TGS

et al., 1990; Gac et al., 2016). The influence of structural inheritance generally decreases drastically during later rift phases, and thermal and structural effects often control final rift geometries (Naliboff et al., 2020). This may explain why reactivation occurred along the Terningen Fault Complex instead of the proposed more easterly second detachment.

A lack of deep penetrating offshore wells leaves seismic facies analysis and interpretation as the only tool for constraining Carboniferous strata within the study area. The Mississippian Billefjorden Group and the Pennsylvanian Gipsdalen Group are present across the SW Barents Sea (Braathen et al., 2012; Gudlaugsson et al., 1998; Larssen et al., 2005; Smyrak-Sikora et al., 2019). Extrapolation

of interpretations by Hassaan et al. (2019) indicates a Mississippian hiatus within the study area, which presumably only accommodate wedge-shaped Pennsylvanian deposits (Figures 3 and 10). The hiatus may be attributed to either local uplift and erosion, or that the marine transgression never reached the Ringsel Ridge. As footwall uplift is suggested to have occurred within the Ringsel Ridge in response to Devonian movements along the Fingerdjupet detachment, we favour the latter interpretation. The interpreted accumulations of SF2-4 correlate with the magnetic anomaly response in the region (Figure 9) and substantiate the model presented in Figure 8. We interpret this to be indicative of isostatic rebound during rifting, which in turn may have exerted control on Carboniferous sedimentation on the Bjarmeland Platform.

6 | CONCLUSIVE REMARKS

This study provides the first integrated account of Caledonian deformation and post-Caledonian detachment faulting in the central SW Barents Sea. Through interpretation of 2D and 3D seismic reflection data, correlated with published analog studies on outcrops and potential field data, we advocate the following:

- Deep-seated shear zones in the metamorphic basement can be ascribed to extensional collapse of the Caledonian orogeny. They were reactivated during subsequent rift phases and exerted control on the structural evolution of the Fingerdjupet Subbasin and to some extent adjacent areas through Late Paleozoic and Mesozoic times.
- Post-Caledonian disintegration ultimately led to two interacting but subsequent, east-stepping detachments with associated exhumation of core complexes. The second detachment was abandoned during Late Paleozoic and Mesozoic rift episodes when deformation again localised along the Fingerdjupet detachment as a response to crustal thinning in the western part of the SW Barents Sea.
- The Fingerdjupet Subbasin in the central SW Barents Sea overlies a Mid Paleozoic supradetachment basin bounded by metamorphic core complexes and a detachment recording a minimum displacement of 22 km. The proposed supradetachment basin likely contains erosional products from the Caledonian mountain chain, and its sedimentary distribution was controlled by isostatically induced along-strike topographic variations along the detachment fault.

ACKNOWLEDGEMENTS

This is a publication of the Suprabasins project supported by AkerBP, Spirit Energy, Equinor and Lundin Energy

Norway and funded by the Research Council of Norway (# 295208). We thank the NGU Geophysics Department for providing TDR filtered magnetic anomaly maps and TGS for providing and allowing us to publish seismic data. Schlumberger is acknowledged for providing the University of Oslo and Norwegian University of Science and Technology with academic software licenses for Petrel. We thank Dora Marín, Chris Morley and Thomas Phillips for their constructive reviews and gratefully acknowledge invaluable discussions with Muhammad Hassaan.

PEER REVIEW

The peer review history for this article is available at <https://publons.com/publon/10.1111/bre.12631>.

DATA AVAILABILITY STATEMENT

The data that support the findings of this study are available from TGS. Restrictions apply to the availability of these data, which were used under license for this study. Data are available from the author(s) with the permission of TGS.

ORCID

Julie L. S. Gresseth  <https://orcid.org/0000-0001-8886-0168>

Alvar Braathen  <https://orcid.org/0000-0002-0869-249X>

Christopher S. Serck  <https://orcid.org/0000-0002-8829-0270>

Jan Inge Faleide  <https://orcid.org/0000-0001-8032-2015>

Per Terje Osmundsen  <https://orcid.org/0000-0001-9814-2370>

REFERENCES

- Andersen, T. B., Osmundsen, P. T., & Jolivet, L. (1994). Deep crustal fabrics and a model for the extensional collapse of the southwest Norwegian Caledonides. *Journal of Structural Geology*, 16(9), 1191–1203. [https://doi.org/10.1016/0191-8141\(94\)90063-9](https://doi.org/10.1016/0191-8141(94)90063-9)
- Andersen, T. B., Torsvik, T. H., Eide, E. A., Osmundsen, P. T., & Faleide, J. I. (1999). Permian and Mesozoic extensional faulting within the Caledonides of central south Norway. *Journal of the Geological Society*, 156(6), 1073–1080. <https://doi.org/10.1144/gsjgs.156.6.1073>
- Anell, I., Braathen, A., Olaussen, S., & Osmundsen, P. (2013). Evidence of faulting contradicts a quiescent northern Barents Shelf during the Triassic. *First Break*, 31(6), 67–76. <https://doi.org/10.3997/1365-2397.2013017>
- Anell, I. M., Faleide, J. I., & Braathen, A. (2016). Regional tectono-sedimentary development of the highs and basins of the north-western Barents Shelf. *Norsk Geologisk Tidsskrift*, 96(1), 27–41.
- Bælum, K., & Braathen, A. (2012). Along-strike changes in fault array and rift basin geometry of the Carboniferous Billefjorden Trough, Svalbard, Norway. *Tectonophysics*, 546–547, 38–55. <https://doi.org/10.1016/j.tecto.2012.04.009>
- Baig, I., Faleide, J. I., Jahren, J., & Mondol, N. H. (2016). Cenozoic exhumation on the southwestern Barents Shelf: Estimates and uncertainties constrained from compaction and thermal maturity analyses. *Marine and Petroleum Geology*, 73, 105–130. <https://doi.org/10.1016/j.marpetgeo.2016.02.024>

- Bergh, S. G., Braathen, A., & Andresen, A. (1997). Interaction of basement-involved and thin-skinned tectonism in the Tertiary fold-thrust belt of central Spitsbergen, Svalbard. *AAPG Bulletin*, 81(4), 637–661.
- Bergh, S. G., Maher, H. D., & Braathen, A. (2011). Late Devonian transpressional tectonics in Spitsbergen, Svalbard, and implications for basement uplift of the Sørkapp-Hornsund High. *Journal of the Geological Society*, 168(2), 441–456. <https://doi.org/10.1144/0016-76492010-046>
- Braathen, A., Bælum, K., Maher, H., & Buckley, S. J. (2012). Growth of extensional faults and folds during deposition of an evaporite-dominated half-graben basin; the Carboniferous Billefjorden Trough, Svalbard. *Norwegian Journal of Geology*, 91(3), 137–160.
- Braathen, A., & Erambert, M. (2014). Structural and metamorphic history of the Engebofjellet Eclogite and the exhumation of the Western Gneiss Region, Norway. *Norwegian Journal of Geology*, 94(1), 53–76.
- Braathen, A., Maher, H. D., Jr., Haabet, T. E., Kristensen, S. E., Tørudbakken, B. O., & Worsley, D. (1999). Caledonian thrusting on Bjørnøya: Implications for Palaeozoic and Mesozoic tectonism of the western Barents Shelf. *Norwegian Journal of Geology*, 79(1), 57–68. <https://doi.org/10.1080/002919699433915>
- Braathen, A., Nordgulen, O., Osmundsen, P. T., Andersen, T. B., Solli, A., & Roberts, D. (2000). Devonian, orogen-parallel, opposed extension in the Central Norwegian Caledonides. *Geology*, 28(7), 615–618. [https://doi.org/10.1130/0091-7613\(2000\)028<0615:DOPOEI>2.3.CO2](https://doi.org/10.1130/0091-7613(2000)028<0615:DOPOEI>2.3.CO2)
- Braathen, A., & Osmundsen, P. T. (2020). Extensional tectonics rooted in orogenic collapse: Long-lived disintegration of the Semail Ophiolite, Oman. *Geology*, 48(3), 258–262. <https://doi.org/10.1130/G47077.1>
- Braathen, A., Osmundsen, P. T., & Gabrielsen, R. H. (2004). Dynamic development of fault rocks in a crustal-scale detachment: An example from western Norway. *Tectonics*, 23(4), 1–21. <https://doi.org/10.1029/2003TC001558>
- Braathen, A., Osmundsen, P. T., Maher, H., & Ganerød, M. (2018). The Keisarhjelmen detachment records Silurian-Devonian extensional collapse in Northern Svalbard. *Terra Nova*, 30(1), 34–39. <https://doi.org/10.1111/ter.12305>
- Braathen, A., Osmundsen, P. T., Nordgulen, Ø., Roberts, D., & Meyer, G. B. (2002). Orogen-parallel extension of the Caledonides in northern Central Norway: An overview. *Norwegian Journal of Geology*, 82(4), 225–241.
- Breivik, A. J., Mjelde, R., Grogan, P., Shimamura, H., Murai, Y., & Nishimura, Y. (2005). Caledonide development offshore Svalbard based on ocean bottom seismometer, conventional seismic, and potential field data. *Tectonophysics*, 401(1–2), 79–117. <https://doi.org/10.1016/j.tecto.2005.03.009>
- Brun, J.-P., Sokoutis, D., Tirel, C., Gueydan, F., Van den Driessche, J., & Beslier, M.-O. (2018). Crustal versus mantle core complexes. *Tectonophysics*, 746, 22–45. <https://doi.org/10.1016/j.tecto.2017.09.017>
- Chauvet, A., & Séranne, M. (1994). Extension-parallel folding in the Scandinavian Caledonides: Implications for late-orogenic processes. *Tectonophysics*, 238(1–4), 31–54. [https://doi.org/10.1016/0040-1951\(94\)90048-5](https://doi.org/10.1016/0040-1951(94)90048-5)
- Corfu, F., Gasser, D., & Chew, D. M. (2014). New perspectives on the Caledonides of Scandinavia and related areas: Introduction. *Geological Society Special Publication*, 390(1), 1–8. <https://doi.org/10.1144/SP390.28>
- Cuong, T. X., & Warren, J. (2009). Bach ho field, a fractured granitic basement reservoir, Cuu Long Basin, offshore SE Vietnam: A ‘buried-hill’ play. *Journal of Petroleum Geology*, 32(2), 129–156.
- Doré, A. G. (1995). Barents Sea geology, petroleum resources and commercial potential. *Arctic*, 48(3), 207–221. <https://doi.org/10.14430/arctic1243>
- Faleide, J. I., Bjørlykke, K., & Gabrielsen, R. H. (2015). Geology of the Norwegian continental shelf. In K. Bjørlykke (Ed.), *Petroleum geoscience* (pp. 603–637). Springer. https://doi.org/10.1007/978-3-642-34132-8_25
- Faleide, J. I., Gudlaugsson, S. T., & Jacquart, G. (1984). Evolution of the western Barents Sea. *Marine and Petroleum Geology*, 1(2), 123, IN121, 129, IN125, 137–128, IN124, 136, IN128, 150. [https://doi.org/10.1016/0264-8172\(84\)90082-5](https://doi.org/10.1016/0264-8172(84)90082-5)
- Faleide, J. I., Tsikalas, F., Breivik, A. J., Mjelde, R., Ritzmann, O., Engen, Ø., Wilson, J., & Eldholm, O. (2008). Structure and evolution of the continental margin off Norway and the Barents Sea. *Episodes*, 31(1), 82–91. <https://doi.org/10.18814/epiiugs/2008/v31i1/012>
- Faleide, J., Vagnes, E., & Gudlaugsson, S. (1993). Late mesozoic-cenozoic evolution of the south-western Barents sea in a regional rift shear tectonic setting. *Marine and Petroleum Geology*, 10(3), 186–214. [https://doi.org/10.1016/0264-8172\(93\)90104-Z](https://doi.org/10.1016/0264-8172(93)90104-Z)
- Fazlikhani, H., Fossen, H., Gawthorpe, R. L., Faleide, J. I., & Bell, R. E. (2017). Basement structure and its influence on the structural configuration of the northern North Sea rift. *Tectonics*, 36(6), 1151–1177. <https://doi.org/10.1002/2017TC004514>
- Fossen, H. (2010). Extensional tectonics in the North Atlantic Caledonides: A regional view. *Geological Society Special Publications*, 335, 767–793. <https://doi.org/10.1144/SP335.31>
- Fossen, H., & Cavalcante, G. C. G. (2017). Shear zones—A review. *Earth-Science Reviews*, 171, 434–455. <https://doi.org/10.1016/j.earscirev.2017.05.002>
- Fossen, H., Teyssier, C., & Whitney, D. L. (2013). Transtensional folding. *Journal of Structural Geology*, 56, 89–102. <https://doi.org/10.1016/j.jsg.2013.09.004>
- Friedmann, S. J., & Burbank, D. W. (1995). Rift basins and supradetachment basins: Intracontinental extensional end-members. *Basin Research*, 7(2), 109–127. <https://doi.org/10.1111/j.1365-2117.1995.tb00099.x>
- Gabrielsen, R. H., Færseth, R. B., Jensen, L. N., Kalheim, J. E., & Riis, F. (1990). *Structural elements of the Norwegian continental shelf Part I: The Barents Sea Region* (97882738511478273851141). Norwegian Petroleum Directorate.
- Gac, S., Klitzke, P., Minakov, A., Faleide, J. I., & Scheck-Wenderoth, M. (2016). Lithospheric strength and elastic thickness of the Barents Sea and Kara Sea region. *Tectonophysics*, 691, 120–132. <https://doi.org/10.1016/j.tecto.2016.04.028>
- Gernigon, L., & Brönnner, M. (2012). Late Palaeozoic architecture and evolution of the southwestern Barents Sea: Insights from a new generation of aeromagnetic data. *Journal of the Geological Society*, 169(4), 449–459. <https://doi.org/10.1144/0016-76492011-131>
- Gernigon, L., Brönnner, M., Roberts, D., Olesen, O., Nasuti, A., & Yamasaki, T. (2014). Crustal and basin evolution of the southwestern Barents Sea: From Caledonian orogeny to continental breakup. *Tectonics*, 33(4), 347–373. <https://doi.org/10.1002/2013TC003439>

- Gradstein, F. M., Ogg, J. G., Schmitz, M. B., & Ogg, G. M. (Eds.). (2012). *The geologic time scale 2012*. Elsevier.
- Gudlaugsson, S. T., Faleide, J. I., Johansen, S. E., & Breivik, A. J. (1998). Late Palaeozoic structural development of the South-western Barents Sea. *Marine and Petroleum Geology*, *15*(1), 73–102. [https://doi.org/10.1016/S0264-8172\(97\)00048-2](https://doi.org/10.1016/S0264-8172(97)00048-2)
- Hartz, E., Andresen, A., Martin, M., & Hodges, K. (2000). U-Pb and Ar-40/Ar-39 constraints on the Fjord Region Detachment Zone: A long-lived extensional fault in the central East Greenland Caledonides. *Journal of the Geological Society*, *157*, 795–809.
- Hassaan, M., Faleide, J., Gabrielsen, R., & Tsikalas, F. (2019). *Control of Carboniferous Graben Structures on Evaporite Accumulation and Domes Location in Southeastern Norwegian Barents Sea*. Paper presented at the 81st EAGE Conference and Exhibition 2019.
- Hedin, P., Almqvist, B., Berthet, T., Juhlin, C., Buske, S., Simon, H., Giese, R., Krauß, F., Rosberg, J.-E., & Alm, P.-G. (2016). 3D reflection seismic imaging at the 2.5 km deep COSC-1 scientific borehole, central Scandinavian Caledonides. *Tectonophysics*, *689*, 40–55. <https://doi.org/10.1016/j.tecto.2015.12.013>
- Holm, D. K., Fleck, R. J., & Lux, D. R. (1994). The Death Valley turtlebacks reinterpreted as Miocene-Pliocene folds of a major detachment surface. *The Journal of Geology*, *102*(6), 718–727. <https://doi.org/10.1086/629715>
- Jakobsson, M., Mayer, L., Coakley, B., Dowdeswell, J. A., Forbes, S., Fridman, B., & Rebesco, M. (2012). The international bathymetric chart of the Arctic Ocean (IBCAO) version 3.0. *Geophysical Research Letters*, *39*(12), 1–5. <https://doi.org/10.1029/2012GL052219>
- Johansen, S. E., Ostisy, B. K., Birkeland, Ø., Federovsky, Y. F., Martirosian, V. N., Christensen, O., Cheredeev, S. I., Ignatenkol, E. A., & Margulis, L. S. (1993). Hydrocarbon potential in the Barents Sea region: Play distribution and potential. *Norwegian Petroleum Society Special Publications*, *2*, 273–320. <https://doi.org/10.1016/B978-0-444-88943-0.50024-1>
- Kapp, P., Taylor, M., Stockli, D., & Ding, L. (2008). Development of active low-angle normal fault systems during orogenic collapse: Insight from Tibet. *Geology*, *36*(1), 7–10. <https://doi.org/10.1130/G24054A.1>
- Koehl, J.-B., Bergh, S. G., Henningsen, T., & Faleide, J. I. (2018). Middle to Late Devonian–Carboniferous collapse basins on the Finnmark Platform and in the southwesternmost Nordkapp basin, SW Barents Sea. *Solid Earth*, *9*(2), 341–372. <https://doi.org/10.5194/se-9-341-2018>
- Krabbendam, M., & Dewey, J. F. (1998). Exhumation of UHP rocks by transtension in the Western Gneiss Region, Scandinavian Caledonides. *Geological Society, London, Special Publications*, *135*(1), 159–181. <https://doi.org/10.1144/GSL.SP.1998.135.01.11>
- Larssen, G. B., Elvebakk, G., Henriksen, L. B., Kristensen, S., Nilsson, I., Samuelsen, T., Svånå, T., Stemmerik, L., & Worsley, D. (2005). *Upper Palaeozoic lithostratigraphy of the southern part of the Norwegian Barents Sea* (97882738511478273851141). Norwegian Petroleum Directorate.
- Lavier, L., Buck, W., Poliakov, A., & Lavier, L. (1999). Self-consistent rolling-hinge model for the evolution of large-offset low-angle normal faults. *Geology*, *27*(12), 1127–1130. [https://doi.org/10.1130/0091-7613\(1999\)0272.3.CO2](https://doi.org/10.1130/0091-7613(1999)0272.3.CO2)
- Lenhart, A., Jackson, C.-A.-L., Bell, R. E., Duffy, O. B., Gawthorpe, R. L., & Fossen, H. (2019). Structural architecture and composition of crystalline basement offshore west Norway. *Lithosphere*, *11*(2), 273–293. <https://doi.org/10.1130/L668.1>
- Lister, G. S., & Davis, G. A. (1989). The origin of metamorphic core complexes and detachment faults formed during Tertiary continental extension in the northern Colorado River region, U.S.A. *Journal of Structural Geology*, *11*, 65–94. [https://doi.org/10.1016/0191-8141\(89\)90036-9](https://doi.org/10.1016/0191-8141(89)90036-9)
- Little, T., Hacker, B., Gordon, S., Baldwin, S., Fitzgerald, P., Ellis, S., & Korchinski, M. (2011). Diapiric exhumation of Earth's youngest (UHP) eclogites in the gneiss domes of the D'Entrecasteaux Islands, Papua New Guinea. *Tectonophysics*, *510*(1–2), 39–68. <https://doi.org/10.1016/j.tecto.2011.06.006>
- Miller, M. B., & Pavlis, T. L. (2005). The Black Mountains turtlebacks: Rosetta stones of Death Valley tectonics. *Earth-Science Reviews*, *73*(1–4), 115–138. <https://doi.org/10.1016/j.earscirev.2005.04.007>
- Muñoz-Barrera, J. M., Rotevatn, A., Gawthorpe, R. L., Henstra, G. A., & Kristensen, T. B. (2020). The role of structural inheritance in the development of high-displacement crustal faults in the necking domain of rifted margins: The Klakk Fault Complex, Frøya High, offshore mid-Norway. *Journal of Structural Geology*, *140*, 104163. <https://doi.org/10.1016/j.jsg.2020.104163>
- Naliboff, J., Glerum, A., Brune, S., Péron-Pinvidic, G., & Wrona, T. (2020). Development of 3-D rift heterogeneity through fault network evolution. *Geophysical Research Letters*, *47*(13), e2019GL086611. <https://doi.org/10.1029/2019GL086611>
- NPDF—Norwegian Petroleum Directorate Factpages. (2020). <http://factpages.npd.no>
- Olesen, O., Brønner, M., Ebbing, J., Gellein, J., Gernigon, L., Koziel, J., Lauritsen, T., Myklebust, R., Pascal, C., Sand, M., Solheim, D., & Usov, S. (2010). New aeromagnetic and gravity compilations from Norway and adjacent areas: Methods and applications. *Geological Society, London, Petroleum Geology Conference series*, *7*(1), 559–586. <https://doi.org/10.1144/0070559>
- Osmundsen, P., & Andersen, T. (2001). The middle Devonian basins of western Norway: Sedimentary response to large-scale transtensional tectonics? *Tectonophysics*, *332*(1–2), 51–68. [https://doi.org/10.1016/S0040-1951\(00\)00249-3](https://doi.org/10.1016/S0040-1951(00)00249-3)
- Osmundsen, P., Andersen, T., Markussen, S., & Svendby, A. (1998). Tectonics and sedimentation in the hangingwall of a major extensional detachment: The Devonian Kvamshesten Basin, western Norway. *Basin Research*, *10*(2), 213–234. <https://doi.org/10.1046/j.1365-2117.1998.00064.x>
- Osmundsen, P. T., Braathen, A., Gresseth, J. L. S., Midtkandal, I., Poyatos-More, M., Péron-Pinvidic, G., & Serck, C. S. (2021, January). *Detachment faulting, successive incision and supra-detachment basin evolution in large-magnitude extensional systems—Examples from analogue studies and the Mid-Norwegian margin*. Paper presented at the 34th Geological Winter Meeting, digital conference. <https://www.geologi.no/konferanser/vinterkonferanser/item/1108-abstractsvk21>
- Osmundsen, P. T., Braathen, A., Nordgulen, Ø., Roberts, D., Meyer, G., & Eide, E. (2003). The Devonian Nesna shear zone and adjacent gneiss-cored culminations, North-Central Norwegian Caledonides. *Journal of the Geological Society*, *160*(1), 137–150. <https://doi.org/10.1144/0016-764901-173>
- Osmundsen, P. T., & Ebbing, J. (2008). Styles of extension offshore mid-Norway and implications for mechanisms of crustal thinning at passive margins. *Tectonics*, *27*(6), 1–25. <https://doi.org/10.1029/2007TC002242>

- Osmundsen, P. T., Eide, E. A., Haabesland, N. E., Roberts, D., Andersen, T. B., Kendrick, M., Bingen, B., Braathen, A., & Redfield, T. F. (2006). Kinematics of the Høybakken detachment zone and the Møre-Trøndelag Fault Complex, central Norway. *Journal of the Geological Society*, *163*, 303–318. <https://doi.org/10.1144/0016-764904-129>
- Osmundsen, P. T., & Péron-Pinvidic, G. (2018). Crustal-Scale Fault Interaction at Rifted Margins and the Formation of Domain-Bounding Breakaway Complexes: Insights from Offshore Norway. *Tectonics*, *37*(3), 935–964. <https://doi.org/10.1002/2017TC004792>
- Osmundsen, P. T., Peron-Pinvidic, G., & Bunkholt, H. (2020). Rifting of collapsed orogens: Successive incision of continental crust in the proximal margin offshore Norway. *Tectonics*, *40*(2). <https://doi.org/10.1029/2020TC006283>
- Otto, S. C., & Bailey, R. (1995). Tectonic evolution of the northern Ural Orogen. *Journal of the Geological Society*, *152*, 903–906. <https://doi.org/10.1144/GSL.JGS.1995.152.01.03>
- Phillips, T. B., Jackson, C. A. L., Bell, R. E., Duffy, O. B., & Fossen, H. (2016). Reactivation of intrabasement structures during rifting: A case study from offshore southern Norway. *Journal of Structural Geology*, *91*(C), 54–73. <https://doi.org/10.1016/j.jsg.2016.08.008>
- Platt, J. P., Behr, W. M., & Cooper, F. J. (2015). Metamorphic core complexes: Windows into the mechanics and rheology of the crust. *Journal of the Geological Society*, *172*(1), 9–27. <https://doi.org/10.1144/jgs2014-036>
- Reynolds, S. J., & Lister, G. S. (1990). Folding in mylonitic zones in Cordilleran metamorphic core complexes: Evidence from near the mylonitic front. *Geology*, *18*(3), 216–219.
- Ritzmann, O., & Faleide, J. I. (2007). Caledonian basement of the western Barents Sea. *Tectonics*, *26*(5), 1–20. <https://doi.org/10.1029/2006TC002059>
- Seiler, C., Quigley, M. C., Fletcher, J., Phillips, D., Gladow, A., & Kohn, B. (2013). Stratigraphy and Ar-40/Ar-39 geochronology of the Santa Rosa basin, Baja California: Dynamic evolution of a constrictional rift basin during oblique extension in the Gulf of California. *Basin Research*, *25*(4), 388–418. <https://doi.org/10.1111/bre.12004>
- Serck, C. S., & Braathen, A. (2019). Extensional fault and fold growth: Impact on accommodation evolution and sedimentary infill. *Basin Research*, *31*(5), 967–990. <https://doi.org/10.1111/bre.12353>
- Serck, C. S., Braathen, A., Olaussen, S., Osmundsen, P. T., Midtkandal, I., van Yperen, A. E., & Indrevær, K. (2021). Supradetachment to rift basin transition recorded in continental to marine deposition; Paleogene Bandar Jissah Basin, NE Oman. *Basin Research*, *33*(1), 544–569. <https://doi.org/10.1111/bre.12484>
- Serck, C. S., Faleide, J. I., Braathen, A., Kjølhamar, B., & Escalona, A. (2017). Jurassic to Early Cretaceous basin configuration(s) in the Fingerdjupet Subbasin, SW Barents Sea. *Marine and Petroleum Geology*, *86*, 874–891. <https://doi.org/10.1016/j.marpetgeo.2017.06.044>
- Shulgin, A., Faleide, J. I., Mjelde, R., Breivik, A., & Huisman, R. (2020). Crustal domains in the Western Barents Sea. *Geophysical Journal International*, *221*(3), 2155–2169. <https://doi.org/10.1093/gji/ggaa112>
- Smelror, M., Petrov, O. V., Larssen, G. B., & Werner, S. C. (2009). *Atlas: Geological history of the Barents Sea*. Geological Survey of Norway.
- Smyrak-Sikora, A., Johannessen, E. P., Olaussen, S., Sandal, G., & Braathen, A. (2019). Sedimentary architecture during Carboniferous rift initiation—The arid Billefjorden Trough, Svalbard. *Journal of the Geological Society*, *176*(2), 225–252. <https://doi.org/10.1144/jgs2018-100>
- Souche, A., Beyssac, O., & Andersen, T. B. (2012). Thermal structure of supra-detachment basins: A case study of the Devonian basins of western Norway. *Journal of the Geological Society*, *169*(4), 427–434. <https://doi.org/10.1144/0016-76492011-155>
- Trice, R., Hiorth, C., & Holdsworth, R. (2019). Fractured basement play development on the UK and Norwegian rifted margins. *Geological Society, London, Special Publications*, *495*, SP495-2018-2174. <https://doi.org/10.1144/SP495-2018-174>
- Vetti, V., & Fossen, H. (2012). Origin of contrasting Devonian supradetachment basin types in the Scandinavian Caledonides. *Geology*, *40*(6), 571–574. <https://doi.org/10.1130/g32512.1>
- Wang, C., Okaya, D. A., Ruppert, C., Davis, G. A., Guo, T., Zhong, Z., & Wenk, R. (1989). Seismic reflectivity of the Whipple Mountain shear zone in southern California. *Journal of Geophysical Research*, *94*(B3), 2989–3005. <https://doi.org/10.1029/JB094iB03p02989>
- Whitney, D. L., Teysier, C., Rey, P., & Buck, W. (2013). Continental and oceanic core complexes. *Geological Society of America Bulletin*, *125*(3–4), 273–298. <https://doi.org/10.1130/B30754.1>
- Wiest, J. D., Wrona, T., Bauck, M. S., Fossen, H., Gawthorpe, R. I., Osmundsen, P. T., & Faleide, J. I. (2020). From Caledonian collapse to North Sea Rift: The Extended history of a metaorphic core complex. *Tectonics*, *39*, 1–15. <https://doi.org/10.1029/2020TC006178>

SUPPORTING INFORMATION

Additional supporting information may be found in the online version of the article at the publisher's website.

How to cite this article: Gresseth, J. L. S., Braathen, A., Serck, C. S., Faleide, J. I., & Osmundsen, P. T. (2021). Late Paleozoic supradetachment basin configuration in the southwestern Barents Sea—Intrabasement seismic facies of the Fingerdjupet Subbasin. *Basin Research*, *00*, 1–20. <https://doi.org/10.1111/bre.12631>